Charmonium: Comparison with experiment

E. Eichten,* K. Gottfried, T. Kinoshita, K. D. Lane,* and T. M. Yan

Laboratory of Nuclear Studies, Cornell University, Ithaca, New York 14853
(Received 25 June 1979)

The charmonium model, formulated in detail in an earlier publication, is compared in a comprehensive fashion with the data on the ψ family. The parameters of the "naive" model, in which the system is described as a $c\bar{c}$ pair, are determined from the observed positions of ψ, ψ', and the P states. The model then yields a successful description of the spectrum of spin-triplet states above the charm threshold. It also accounts for the ratio of the leptonic widths of ψ' and ψ. When the $c\bar{c}$ potential is applied to the Υ family, it accounts, without any readjustment of parameters, for the positions of the $2S$ and $3S$ levels and for the leptonic widths of Υ and Υ' relative to that of ψ. The model does not give acceptable values of the absolute leptonic widths, a shortcoming which is ascribed to large quantum-chromodynamic corrections to the van Royen–Weisskopf formula. The calculated $E1$ rates are about twice the values observed in the ψ family. This naive model is also extended with considerable success to mesons composed of one heavy and one light quark. A significant extension of the model is achieved by incorporating coupling to charmed-meson decay channels. This gives a satisfactory understanding of $\psi(3772)$ as the 1^3D_1 $c\bar{c}$ state, mixed via open and closed decay channels to 2^3S. The model has decay amplitudes that are oscillatory functions of the decay momentum; these oscillations are a direct consequence of the radial nodes in the $c\bar{c}$ parent states. These amplitudes provide a qualitative understanding of the observed peculiar branching ratios into various charmed-meson channels near the resonance at 4.03 GeV, which is assigned to 3^3S. The coupling of the $c\bar{c}$ states below the charm threshold to closed decay channels modifies the bound states and leads to reduction of about 20% in $E1$ rates in comparison to those of the naive model.

I. INTRODUCTION

This paper is devoted to a comparison between the charmonium model and the data on the J/ψ family. In view of recent and anticipated developments concerning the Υ family, we also pay some heed to the extension of the model to heavier quark-antiquark systems. In an Appendix, we also provide a discussion of mesons composed of one heavy quark and one light quark. A complete description of the model, and of the associated formalism, was given in an earlier paper,[1] which shall be cited as I hereafter. We emphasize that, with but few exceptions, our discussion will be based on our own work of recent years; for more comprehensive accounts of this new branch of hadronic spectroscopy, the reader is referred to the review literature.[2-8]

II. THE NAIVE $Q\bar{Q}$ MODEL

The naive model assumes that the ψ and Υ levels are adequately described by the degrees of freedom of a heavy quark Q and its antiparticle $\bar{Q}$. It is characterized by the parameters that appear in the static $Q\bar{Q}$ potential, and the mass m_Q of Q. The fabrication of static $Q\bar{Q}$ potentials has grown apace[5,8,9] since the discovery of Υ, but a detailed comparison of all these models falls outside the scope of this article. Except for some general remarks that apply to all these potentials, we shall confine ourselves to the comparison of data with the predictions of the familiar linear plus Coulomb potential model

$$V(r) = -\frac{\kappa}{r} + \frac{r}{a^2}, \qquad (2.1)$$

supplemented by the standard assumption that the sole flavor dependence of the gross level structure stems from the quark mass.

A. New determination of model parameters

When the model (2.1) was first proposed, only ψ and ψ' were known. Consequently one had to fix the parameters from the ψ-ψ' mass difference and the leptonic widths, subject to the general requirement that $(v/c)^2$ remain "small." Today we have a far richer body of data, and while much of it was predicted by the model, only nostalgia would justify the original strategy for fixing the parameters of the model. Instead, one should determine the parameters from those phenomena that are reliably measured and where one has most confidence in the theoretical computation. While there is little controversy concerning the data, there is much room for debate about the reliability of the different parts of the theoretical framework. For that reason, we start with the following summary of our views concerning the status of the theory:

(1) The use of a Schrödinger equation with a static potential is only justified if the resultant motion is nonrelativistic.

(2) The *raison d'être* for such a nonrelativistic

potential model is the computation of energy levels, and one should therefore require that the model gives the best possible fit to the excitation spectrum.

(3) Despite much effort,[8] our theoretical understanding of relativistic corrections, and of spin-dependent forces, is still quite limited.

(4) The regime of small $Q\overline{Q}$ separation, where asymptotic freedom prevails, plays little role in the ψ family, and is still of secondary importance in the Υ family; consequently, the well-known formulas for $Q\overline{Q}$ annihilation into leptons and hadrons may not be reliable, and the Coulombic parameter κ in (2.1) is only some effective strength of the short-range potential which is not necessarily related to the running coupling constant.

We now turn to the data bearing these last remarks in mind. First we note that only the spin-triplet members of the ψ family are firmly established. When we fit a model to the known levels, we automatically incorporate the $S=1$ portion of the hyperfine interaction $H_{hf}^{(1)}$ in the effective potential V. If QED is any guide, $H_{hf}^{(1)}$ is more singular as $r \to 0$ than the central potential, and therefore the short-distance part of V is the sum of $H_{hf}^{(1)}$ and the "true" short-distance central potential V_0. This is another reason why κ does not have a straightforward relation to the α_s of quantum chromodynamics (QCD).

Second, the ^3P splitting, while being as large as $\sim\frac{1}{4}$ of the ψ'-ψ separation, is small enough so that one expects the measured center of gravity of the ^3P multiplet to agree quite closely with the lowest P level of the effective $S=1$ potential. In assuming this we ignore spin-independent corrections to the nonrelativistic spectrum. These fall into two categories: one that is independent of the interaction (i.e., the p^4 term), and others that depend on it. The latter can only be calculated reliably from a field-theoretic description of the system, something that we do not possess. Nevertheless, we have examined this question by using the naive Breit-Hamiltonian approach, and our potential (2.1). After terms that behave like $1/r$ are absorbed by a redefinition of κ, we find that the total relativistic spin-independent correction to the 1^3S-1^3P splitting is only 30 MeV. While this is a model-sensitive result, it does lend support to the strategy for determining the model parameters that we shall adopt.

On the basis of the foregoing remarks, we conclude that it is best to use the relative positions of ψ, ψ', and the ^3P center of gravity (c.o.g.) as two conditions to restrict the three parameters m_c, κ, and a that characterize the ψ family. We are then left with one unknown combination of these parameters, and we choose this to be v_ψ^2, the mean-square velocity in the $1S$ state. The dependence of m_c, κ, and a on v_ψ^2 is shown in Fig. 1. The remaining observable quantities, in particular the various transition rates, can then be computed as functions of v_ψ^2. If the model were actually capable of giving a fit to all the data, these quantities would all lead to the same $small$ value of v_ψ^2.

Unfortunately, we are not in this happy situation. This is illustrated by Fig. 2, which shows the ground-state leptonic width $\Gamma(\psi \to e^+e^-)$ and one of the $E1$ rates $\Gamma(\psi' \to \gamma^3P_0)$ as functions of v_ψ^2. Both of these curves are computed from the naive nonrelativistic rate formulas. The measured values of $\Gamma(\psi \to e^+e^-)$ and $\Gamma(\psi' \to \gamma^3P_0)$ are also shown in Fig. 2. We note that there is no value of v_ψ^2 that yields a fit to both rates: The $E1$ rate is small, so to say, and requires low-velocity motions, but such low velocities give far too large an annihilation probability.

This conundrum is, to a greater or lesser extent, common to all the models. The logarithmic potential,[10] which gives a good fit to the ψ spectrum, leads to values of v_ψ^2 that we find unacceptably large, and also $E1$ rates that are uncomfortably large. Models[11] which use a modified Coulomb interaction that supposedly accounts for the running coupling constant of QCD are, in the final analysis, quite similar to our model (2.1) with a
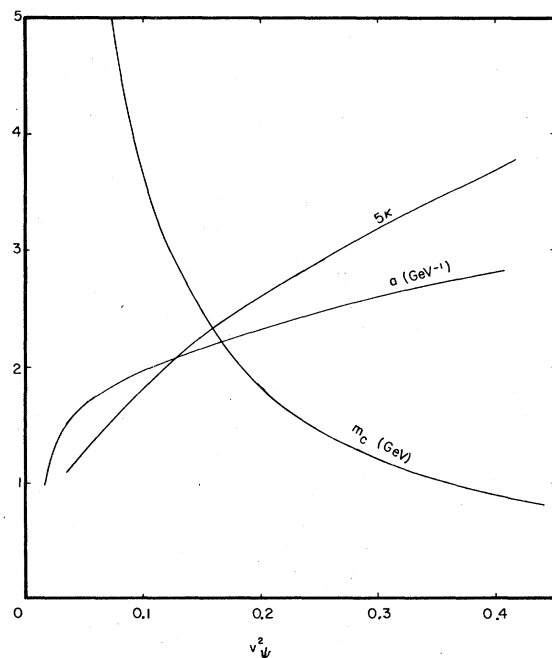
FIG. 1. The parameters m_c, κ, and a as functions of the mean-square velocity v_ψ^2 of ψ. Two energy differences are held fixed at their experimental values: $E(2S) - E(1S) = m(\psi') - m(\psi)$, and $E(1P) - E(1S) = m$(c.o.g. of χ_J) $- m(\psi)$. For the sake of clarity, 5κ is plotted.
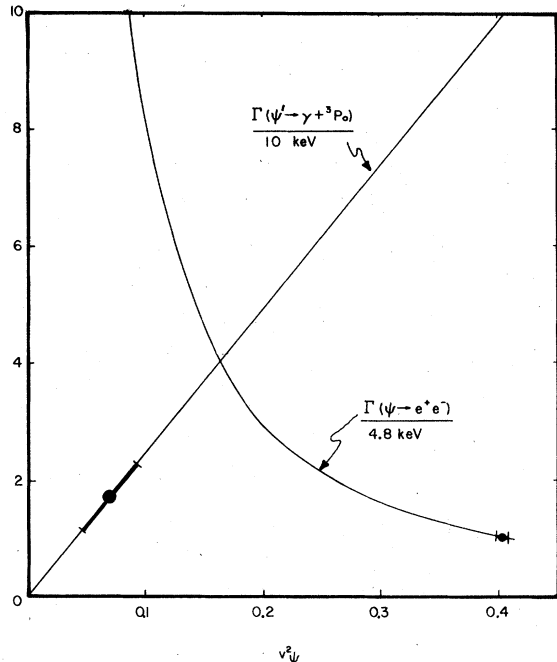
FIG. 2. The $E1$ transition rate $\Gamma(\psi' \to \gamma + {}^3P_0)$ and the electronic width $\Gamma(\psi \to e^+e^-)$ as functions of $v_\psi{}^2$. The energy differences $E(2S) - E(1S)$ and $E(1P) - E(1S)$ are held fixed as in Fig. 1. The measured values, together with their errors, are indicated.

large value of κ. The "modified" linear plus Coulomb model of Quigg and Rosner,[10] which is fixed by the requirement $m(\Upsilon') - m(\Upsilon) = m(\psi') - m(\psi)$, is also quite close to our model. Consequently all of these models suffer from the affliction depicted in Fig. 2.

Most authors escape from the dilemma by requiring their model to fit $\Gamma(\psi \to e^+e^-)$, and do not consider the fact that that choice makes their model highly relativistic. As stated repeatedly, we find this quite unsatisfactory. In our view it is sounder to choose a sensibly small value of $v_\psi{}^2$, and to openly admit that there is some missing link which prevents one from accounting for the *absolute* values of the leptonic widths. That this is a defensible position is supported by arguments[12,5] that cast doubt on the reliability of the van Royen-Weisskopf formula [Eq. (2.2) of I] for the leptonic width. Thus, Celmaster[12] has observed that in positronium the amplitude for $e^+e^- \to \gamma$ has a relativistic correction of order e^2, and that when this correction is straightforwardly modified for color (and $e^2/4\pi$ is replaced by α_s) a very large suppression results. Furthermore, there is little question that this correction has a direct analog in QCD. What is not clear is whether other higher-order corrections are of comparable importance. Adopting the most naive translation

from QED to QCD one finds[12]

$$\Gamma(e^+e^-) = \Gamma_0(e^+e^-)\left(1 - \frac{16}{3\pi}\,\alpha_s\right), \qquad (2.2)$$

where

$$\Gamma_0(e^+e^-) = \frac{16\pi e_Q{}^2 \alpha^2}{M_n{}^2}\,|\psi_n(0)|^2 \qquad (2.3)$$

is the van Royen-Weisskopf width. The correction factor in (2.2) is not, as we have said, reliably known, but it does arise from highly virtual quark pairs, and is therefore insensitive to the particular $Q\bar{Q}$ state in question. Consequently the *ratios* of leptonic widths within *one* $Q\bar{Q}$ family should still be well described by the model, even if the absolute widths are not. Furthermore, if the correction factor in (2.2) varies slowly with quark mass, the rate of $\Upsilon \to e^+e^-$ relative to $\psi \to e^+e^-$ can also be computed with reasonable confidence.

Having said all this, we must finally choose a value of $v_\psi{}^2$ so as to fix all our parameters. This choice is, of necessity, somewhat arbitrary and subjective. Our decision is guided by the observation that the charmed-quark mass should be close to the lowest charmed-meson mass. (Our estimates also show that the mass of the b quark is close to that of the lightest B meson; see discussion in Sec. IID.) We choose $v_\psi{}^2 = 0.20$; the sensitivity of the final results to the precise value of $v_\psi{}^2$ will be described below. With the help of Appendix A of I, the model parameters corresponding to this $v_\psi{}^2$ are then found to be

$$\begin{aligned}
A: \quad m_c &= 1.84 \text{ GeV}, \\
a &= 2.34 \text{ GeV}^{-1}, \\
\kappa &= 0.52, \\
\lambda &= \kappa(m_c a)^{2/3} = 1.37.
\end{aligned} \qquad (2.4)$$

The potential itself is plotted in Fig. 3. As one sees, it is not very different from the logarithmic potential for intermediate distances, though it is appreciably different at larger r. Consequently the higher levels predicted by the two potentials differ considerably.

According to Fig. 2, $v_\psi{}^2 = 0.20$ gives a value of $\Gamma(\psi \to e^+e^-)$ which is three times the observed value if one uses the naive rate formula (2.3). For popular values of α_s the correction factor in (2.2) ranges from $\frac{1}{3}$ to $\frac{1}{2}$, and therefore the ground-state wave function corresponding to (2.4) may well be capable of accounting for the observed leptonic width once the relativistic and dynamic corrections are incorporated. In fact, if we identify κ with $\frac{4}{3}\alpha_s$, our choice of κ in (2.4) gives a correction factor which reproduces the observed leptonic width of ψ $[\Gamma_{ee}(\psi) = 4.8 \text{ keV}]$.
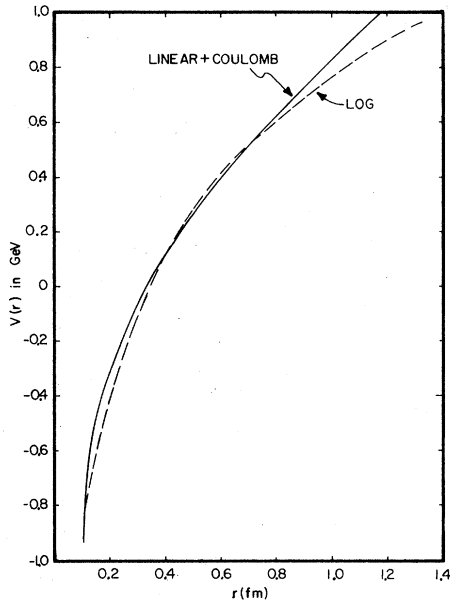
FIG. 3. Comparison of the linear plus Coulomb potential and the logarithmic potential. The parameters of the former are given in Eq. (2.4), while $V_{log}(r)$ = 0.731 GeV × ln$r$. The two potentials are arbitrarily made to coincide at $r = 0.47$ fm, the mean-square radius of the 1S state in our model.

For the record, we should compare parameter set A of Eq. (2.4) with our earlier set, which we call B. The latter did *not* use the ^3P c.o.g. as an input, and instead used the observed value of $\Gamma(\psi \to e^+e^-)$ plus 1 standard deviation. Set B was[2,13-15]

B: $m_c = 1.65$ GeV ,

    $a = 2.07$ GeV^{-1} ,

    $\kappa = 0.30$,   (2.5)

    $\lambda = 0.68$.

Note that λ, the dimensionless parameter that characterizes the strength of the Coulombic interaction, is twice as big with our new parameter set A.

B. Comparison with data on spin-triplet ψ states

Having settled on the parameters, we can now compare the other consequences of the model with experiment.[16] Unless stated otherwise, results quoted henceforth stem from parameter set A.

First we recall that the *ratio* of leptonic widths is not expected to suffer from the uncertainties discussed in connection with Eq. (2.2). We express this ratio as a ratio of squares of wave functions at the origin. We find

$$\left| \frac{\psi_{2S}(0)}{\psi_{1S}(0)} \right|^2 = 0.64 . \qquad (2.6a)$$

Assuming that 1^3D mixes only with 2^3S, we can compare this to

$$\left(\frac{m(\psi')}{m(\psi)} \right)^2 \frac{\Gamma(\psi' \to e^+e^-)}{\Gamma(\psi \to e^+e^-)} \ \sec^2\theta$$

$$= \begin{cases} 0.73 \pm 0.11 & (\text{SLAC-LBL}), \\ 0.68 \pm 0.20 & (\text{DELCO}), \end{cases} \qquad (2.6b)$$

where θ is the 2S-1D mixing angle inferred[17,18] from $\psi(3772)$. The agreement is good—considerably better than with our old parameter set B, where (2.6a) is replaced by 0.81. We emphasize that the ratio (2.6a) is independent of the choice of v_ψ^2: It depends only on the parameter λ, which is fixed by the ratio of the mass splittings $m(\psi') - m(\psi)$ and $m(1P) - m(\psi)$.

The $E1$ rates for $\psi' \to \gamma\,^3P_J$ are compared with experiments in Table I. We should like to take this opportunity to correct an error in Paper I, namely, Eq. (A7) should have read

$$E_{if} = \frac{3}{2} \frac{1}{K} \int_0^\infty d\rho \left[\left(1 + \frac{k}{4m_c} \right) u_f(\rho)[K\rho j_0(K\rho) \right.$$

$$- j_1(K\rho)]u_i(\rho)$$

$$\pm \frac{k}{4m_c} [J(J+1) - 4]u_f(\rho)u_i(\rho)j_1(K\rho)$$

$$\left. + \frac{k}{2m_c} u_f(\rho)\rho[\partial u_i(\rho)/\partial\rho]j_1(K\rho) \right] , \qquad (2.7)$$

where the upper (lower) sign applies to $^3S_1 \to \gamma\,^3P_J$ ($^3P_J \to \gamma\,^3S_1$) and $K = \frac{1}{2}ka(m_ca)^{-1/3}$. The difference between the rates computed with this elaborate

TABLE I. Rates of $E1$ transitions of ψ' and χ states in naive model.

Transitions	Γ_{E1} (keV) [a]	Γ_{E1} (keV) [b]	Experiment Branching ratio (%) [c]
$\psi' \to \gamma + \chi_0$	50.0	16 ± 9	6.8 ± 0.6
$\to \gamma + \chi_1$	45.3	16 ± 8	7.1 [d]
$\to \gamma + \chi_2$	28.9	16 ± 9	6.9 ± 0.5
$\chi_0 \to \gamma + \psi$	141		
$\chi_1 \to \gamma + \psi$	289		
$\chi_2 \to \gamma + \psi$	398		

[a] Photon energies are computed from the experimental masses of the χ_J states, 3.415, 3.510, and 3.550 GeV for $J = 0$, 1, and 2, respectively, which are identified with 1^3P_J states.

[b] Reference 16.

[c] Reference 21.

[d] We give no error here because only relative branching ratios are measured (see Ref. 21).

TABLE II. $c\bar{c}$ bound states in naive model, and their properties. Parameters used are m_c = 1.84 GeV, a = 2.34 GeV^{-1}, and κ = 0.52.

State	Mass (GeV)	Γ_{ee} (keV) [b]	$\left\langle \dfrac{v^2}{c^2} \right\rangle$	$\langle r^2 \rangle^{1/2}$ (fm)	Candidate
$1S$	3.095 [a]	4.8	0.20	0.47	$\psi(3095)$
$1P$	3.522 [a]		0.20	0.74	$\chi_{0,1,2}(3522 \pm 5)$
$2S$	3.684 [a]	2.1	0.24	0.96	$\psi'(3684)$
$1D$	3.81		0.23	1.0	$\psi'(3772)$ [c]
$3S$	4.11	1.5	0.30	1.3	$\psi(4028)$
$2D$	4.19		0.29	1.35	$\psi(4160)$ [d]
$4S$	4.46	1.1	0.35	1.7	$\psi(4414)$
$5S$	4.79	0.8	0.40	2.0	

[a] Input.
[b] Correction factor $(1 - 4\kappa/\pi) = 0.341$ is included.
[c] See Ref. 18.
[d] See Ref. 20.

formula, and the naive one which holds in the limit $K \rightarrow 0$, are marginal ($\lesssim 7\%$), and are not incorporated in Table I. As we see from Table I, our new parameter set does not give any improvement over the predictions[13] that preceded the discovery of the P states.

We shall not discuss the $\gamma\gamma$ cascades as their combined branching ratios involve two independent theoretical factors—the hadronic widths of the P states, and the $E1$ rates for $^3P_J \rightarrow \gamma\psi$. We list the $E1$ rates in Table I, but we have nothing to add to the existing discussions[3] of P-state hadronic widths.

Finally, we come to the spectrum above charm threshold. Here tradition requires us to attempt the somewhat questionable exercise of correlating cross-section bumps with the naive level scheme, even though the latter ignores coupling to decay channels. Table II gives the naive positions of the lowest ^3S and ^3D states above threshold, and compares this with the structures observed at SPEAR and DORIS. There is a rather satisfying correspondence between the model and observation. Here, it should be noted, is one place where there is a real difference between the logarithmic and linear confinement potential. In the former the level density is rather large than the latter, and where we would associate $\psi(4160)$ with 2^3D, the logarithmic model would identify this as 4^3S. The possibility of distinguishing between these assignments will be discussed in Sec. V.

C. Spin-singlet ψ states

With the discovery[18] of $\psi(3772)$ all the low-lying spin triplets expected in the charmonium model have been found. At the moment we have no reliable information about any spin-singlet state. While there have been candidates for both 1^1S [$X(2830)$ observed at DORIS[19]] and 2^1S [$\chi(3450)$ and

$\chi(3600)$ possibly seen[16,20] in $\psi' \rightarrow \gamma\gamma\psi$], their properties disagreed so badly with the model that we have long argued[2,5,6] that they were not the hyperfine partners of ψ and ψ'. The recently announced results from SPEAR[21] confirm this—at this time the ^1S states remain undiscovered. Presumably they lie quite close to ψ and ψ', and are therefore very difficult to observe.[21a]

The rates for allowed $M1$ transitions (which were erroneously given in I, see Errata[1]) are given by

$$\Gamma(\psi' \rightarrow \gamma + \eta_c')/k^3 = \Gamma(\psi \rightarrow \gamma + \eta_c)/k^3$$

$$= \frac{16}{3}\left(\frac{e_c}{2m_c}\right)^2 \alpha$$

$$= 1275 \frac{\text{keV}}{\text{GeV}^3} . \tag{2.8}$$

The rates for hindered $M1$ transitions, such as $\psi' \rightarrow \gamma + \eta_c$, are sensitive to the details of the wave functions and the actual values of the photon energy. We have numerically evaluated the matrix element defined in (2.24) and (2.25) of I. The results of allowed and hindered $M1$ transitions are summarized in Table III. In view of relativistic effects,[22] and other uncertainties, these results must be used with caution. But even as an order of magnitude estimate, it is interesting to note that the transition $\psi' \rightarrow \gamma + \eta_c$ has a branching ratio of ~0.3% for a mass difference of 50–100 MeV between ψ and η_c. Since there should be very little background in the inclusive photon spectrum for a photon energy of ~600 MeV, this transition may be observable.

D. The Υ and still heavier $Q\bar{Q}$ families[21a]

Our parameter set A has the virtue of giving a $\Upsilon' - \Upsilon$ splitting that is close to the observed[23-25]

TABLE III. Naive-model $M1$ transition rates of ψ particles. Equation (2.24) of I for the $M1$ transition rate is incorrect; see Erratum (Ref. 1). A factor $\frac{16}{3}$ should have multiplied the formula given there.

Transition	Δm (MeV)		k (MeV)	$S\left(\dfrac{\text{keV}}{\text{GeV}^3}\right)$ [b]	Γ_{M1} (keV)	Branching ratio (%) [c]
$\psi' \to \gamma + \eta_c$ [a]	$\psi - \eta_c =$	50	584		0.56	0.25
	$\psi - \eta_c =$	100	625		0.88	0.40
$\psi \to \gamma + \eta_c$	$\psi - \eta_c =$	50	49.6	1275	0.15	0.23
	$\psi - \eta_c =$	100	98.4	1275	1.23	1.81
$\psi' \to \gamma + \eta'_c$	$\psi' - \eta'_c =$	25	24.9	1275	1.97×10^{-2}	8.5×10^{-3}
	$\psi' - \eta'_c =$	50	49.6	1275	0.15	6.9×10^{-2}
$\eta'_c \to \gamma + \psi$ [a]	$\psi' - \eta'_c =$	25	521		2.67	0.13
	$\psi' - \eta'_c =$	50	499		1.97	0.1

[a] $M1$ matrix elements for these hindered transitions are computed from Eq. (A9) of I with the wave functions of our potential, and the assumed positions of η_c and η'_c.

[b] The strength S is defined by $\Gamma_{M1} = Sk^3$, where k is the photon energy.

[c] The branching ratios are calculated by using the experimental values $\Gamma(\psi') = 225$ keV, $\Gamma(\psi) = 67$ keV, and the theoretical estimate $\Gamma(\eta'_c) = 2$ MeV.

values of 557 ± 5 MeV (555 ± 3 MeV) for any quark mass m_b in the neighborhood of 5 GeV. This is to be contrasted with our old set B, which predicted a separation of only ~430 MeV. What is now clear is that our original prediction[15] was less accurate because in parameter set B the position of ^3P c.o.g. for the $c\bar{c}$ system was too low by 65 MeV.

Given that we now have the correct value of the Υ'-Υ splitting, it would seem appropriate to set down our predictions for the other observable properties of the Υ system.

First we consider the important question of how many ^3S states exist below the Okubo-Zweig-Iizuka (OZI) threshold. The answer entails two ingredients: (i) the mass of the lightest $b\bar{u}$ meson, which we call m_B, and (ii) the mass of Υ itself. As previously noted,[15] m_B is known reliably:

$$m_B = m_D + m_b - m_c + \frac{3}{4}\left(1 - \frac{m_c}{m_b}\right)(m_{D^*} - m_D).$$

(2.9)

Since Υ'' appears to lie below the OZI threshold, $m(\Upsilon'')$ provides a lower limit on m_B. Using the latest fit[20] to the hadronic production data,[26] which takes into account the DORIS values of $m(\Upsilon)$ and $m(\Upsilon')$, one has[26] $m(\Upsilon'') = 10.41 \pm 0.05$ GeV; with $m_c = 1.84$ GeV, this gives $m_b \geq 5.11$ GeV. The absolute mass $m_n(Q\bar{Q})$ of the Υ levels can only be determined as a function of m_Q if one knows the m_Q dependence of

$$\Delta(m_Q) = m_n(Q\bar{Q}) - 2m_Q - E_n(m_Q),$$

(2.10)

where $E_n(m_Q)$ is the appropriate eigenvalue of the Schrödinger equation. We previously[15] gave a fairly detailed discussion of $\Delta(m_Q)$, which led to the conclusion that $\Delta(m_Q)$ should decrease for m_Q

values in the range of present interest (1.5-5 GeV), but increase as one reaches the Coulombic limit. From that observation we infer a (rather soft) upper limit on m_b by setting $\Delta(m_b) = \Delta(m_c) = -0.84$ GeV. This gives $m_b \leq 5.23$ GeV. The value of the quark mass, $m_b = 5.17$ GeV, used in our calculation is the average of the two limits. With $m_b = 5.17$ GeV we find from (2.9)

$$m_B = 5.26 \text{ GeV}.$$

(2.11)

Thus our estimate indicates that Υ'' lies below the OZI threshold of $B\bar{B}$ production by about 100 MeV. We therefore do not expect any further ^3S $b\bar{b}$ bound states.

The $b\bar{b}$ spectrum is given in Table IV, as well as some properties of the various states. We find

$$m(\Upsilon') - m(\Upsilon) = 591 \text{ MeV},$$
$$m(\Upsilon'') - m(\Upsilon) = 936 \text{ MeV},$$

(2.12)

which agree reasonably well with observed values.[26] The states 2^3D and 3^3S are only about 100 MeV apart and S-D mixing may make the 2^3D visible in the e^+e^- annihilation cross section below the $B\bar{B}$ threshold. The 4^3S and 3^3D states are also very close and can mix. Although they are only 150 to 200 MeV above the $B\bar{B}$ threshold, they are not necessarily good "factories" for $B\bar{B}$ production, as is $\psi''(3772)$ for $D\bar{D}$ production. This is because the mass difference between the vector meson B^* and the pseudoscalar B is expected to be

$$m_{B^*} - m_B = \frac{m_c}{m_b}(m_{D^*} - m_D) \cong 50 \text{ MeV}.$$

(2.13)

Thus not only $B\bar{B}$, but $B^*\bar{B} + B\bar{B}^*$, and even $B^*\bar{B}^*$, will also be produced. The 50 MeV photons which accompany the dominant decay mode $B^* \to B\gamma$ may

TABLE IV. Naive-model $b\bar{b}$ bound states and their properties. Parameters used are m_b = 5.17 GeV, a = 2.34 GeV^{-1}, and κ = 0.52.

State	Eigenvalue (MeV)	Mass (GeV)	Γ_{ee} [b] (keV)	$\left\langle \dfrac{v^2}{c^2} \right\rangle$	$\langle r^2 \rangle^{1/2}$ (fm)
1S	0	9.46 [a]	1.25	0.096	0.20
1P	498	9.96		0.065	0.39
2S	591	10.05	0.45	0.076	0.48
1D	747	10.20		0.067	0.53
2P	852	10.31		0.076	0.64
3S	936	10.40	0.31	0.085	0.72
2D	1040	10.50		0.080	0.75
3P	1135	10.60			
4S	1213	10.67	0.25	0.097	0.92
3D	1292	10.75			
5S	1455	10.92			
6S	1675	11.14			

[a] Input.
[b] See text for how these numbers are obtained.

pose a serious problem for detection.

The leptonic widths for the Υ family are also listed in Table IV. For Υ (9.46) the leptonic width is obtained by using the experimental value of $\Gamma_{e^+e^-}(\psi)$ in the formula

$$\frac{\Gamma_{e^+e^-}(\Upsilon)}{\Gamma_{e^+e^-}(\psi)} = \frac{1}{4}\left(\frac{m(\psi)}{m(\Upsilon)}\right)^2 \left|\frac{\psi_\Upsilon(0)}{\psi_\psi(0)}\right|^2, \qquad (2.14)$$

where we have assumed a charge of $\frac{1}{3}$ for the b quark and neglected the variation of the correction factor in Eq. (2.2). The leptonic widths for higher states are obtained from the ratios to $\Gamma_{e^+e^-}(\Upsilon)$. The theoretical values

$$\Gamma_{e^+e^-}(\Upsilon) = 1.25 \pm 0.16 \text{ keV},$$
$$\Gamma_{e^+e^-}(\Upsilon') = 0.45 \pm 0.06 \text{ keV}, \qquad (2.15)$$

agree well with the observed values[22-25]

$$\Gamma_{e^+e^-}(\Upsilon) = 1.2 \pm 0.2 \text{ keV},$$
$$\Gamma_{e^+e^-}(\Upsilon') = 0.33 \pm 0.10 \text{ keV}. \qquad (2.16)$$

The rates of $E1$ transitions among various Υ spin-triplet states are given in Table V.[27] Since the corresponding predicted rates for the ψ family are about a factor of 2 or 3 too big, one can expect similar discrepancies to occur for the Υ family. For ^3S states which can be directly produced in e^+e^- annihilation, the transition rates are only in the keV region. Hence it is likely that these transitions are harder to see than in the case of the ψ family.

$M1$ rates between hyperfine partners should be even smaller than in charmonium, and therefore very difficult to detect; the same holds true for the hindered $M1$ transitions $2^3S_1 \rightarrow 1^1S_0$ and $3^3S_1 \rightarrow 1^1S_0$. The strength of allowed $M1$ transitions is reduced by a factor $[\frac{1}{2}(m_c/m_b)]^2 = 0.03$ from that of (2.8)

for charmonium.

The total widths of the $b\bar{b}$ bound states below the $B\bar{B}$ threshold can be estimated. According to widespread belief based on QCD, the direct decays into light hadrons are mediated by three- or two-gluon annihilation.[28] However, our earlier discussion on the van Royen-Weisskopf formula for the electronic width suggests that QCD radiative cor-

TABLE V. Naive-model $E1$ transition rates of $b\bar{b}$ states. The b quark is assumed to have an electric charge of $-\frac{1}{3}$.

Transition	k (MeV)	E_{if} [a]	S_{if} [b]	Γ_{E1} (keV)
$3^3S_1 \rightarrow 2^3P_J$	84	2.60	1	$0.50(2J+1)$
$3^3S_1 \rightarrow 1^3P_J$	430	0.11	1	$0.12(2J+1)$
$2^3S_1 \rightarrow 1^3P_J$	93	-1.65	1	$0.27(2J+1)$
$2^3P_J \rightarrow 2^3S_1$	259	1.63	1	17
$2^3P_J \rightarrow 1^3S_1$	817	0.25	1	13
$1^3P_J \rightarrow 1^3S_1$	486	0.91	1	36
$2^3P_0 \rightarrow 1^3D_1$	104	-1.77	2	2.8
$2^3P_1 \rightarrow 1^3D_1$	104	-1.77	$\frac{1}{2}$	0.7
$2^3P_1 \rightarrow 1^3D_2$	104	-1.77	$\frac{9}{10}$	2.1
$2^3P_2 \rightarrow 1^3D_1$	104	-1.77	$\frac{1}{50}$	3×10^{-2}
$2^3P_2 \rightarrow 1^3D_2$	104	-1.77	$\frac{9}{50}$	0.4
$2^3P_2 \rightarrow 1^3D_3$	104	-1.77	$\frac{18}{25}$	2.3
$1^3D_{J_i} \rightarrow 1^3P_{J_f}$ [c]	246	1.89		$6.67 S_{if}(2J_f+1)$

[a] E_{if} is the reduced $E1$ matrix element defined in I.
[b] S_{if} is a statistical factor defined in I, and tabulated in Ref. 15.
[c] To obtain rate for a given J_i and J_f, use $S_{if} = S_{fi}$ listed for $2^3P_{J_i} \rightarrow 1^3D_{J_f}$.

rections to these naive formulas may be important. In QED, it is indeed known[29] that the radiative corrections to the three-photon decay rate of ortho-positronium has a very large coefficient multiplying α/π:

$$\Gamma_{3\gamma} \cong \Gamma_0 \left(1 - 10\frac{\alpha}{\pi}\right). \qquad (2.17)$$

This shows the obvious danger of using simple gluonic annihilation formulas for estimating various rates. To minimize the theoretical uncertainty we rewrite the three-gluon annihilation rates in terms of ratios:

$$\Gamma_{3g}(\Upsilon) = 4\frac{\Gamma_{ee}(\Upsilon)}{\Gamma_{ee}(\psi)}\left(\frac{\alpha_s(\Upsilon)}{\alpha_s(\psi)}\right)^3 \Gamma_{3g}(\psi),$$

$$\Gamma_{3g}(\Upsilon'') = \frac{\Gamma_{ee}(\Upsilon'')}{\Gamma_{ee}(\Upsilon)}\left(\frac{\alpha_s(\Upsilon'')}{\alpha_s(\Upsilon)}\right)^3 \Gamma_{3g}(\Upsilon). \qquad (2.18)$$

For the same reason, the rate for the inclusive decay

$$\Upsilon'' \to \text{real } \gamma + \text{light hadrons}$$

is expressed in terms of the ratio[30]

$$\frac{\Gamma_{\gamma gg}(\Upsilon'')}{\Gamma_{3g}(\Upsilon'')} = \frac{36}{5}\frac{\alpha e_Q^2}{\alpha_s(\Upsilon'')}. \qquad (2.19)$$

The rate for decay via a virtual photon is given by

$$\Gamma_{``\gamma''}(\Upsilon'') = \Gamma_{ee}(\Upsilon'')(R_{\text{had}}+3), \qquad (2.20)$$

where the first term, proportional to R_{had}, is the decay into light hadrons due to the second-order electromagnetic interaction, and the second term accounts for decay into e, μ, and τ pairs.

For our estimate we adopt the following values for the ψ family:

$$\Gamma_{3g}(\psi) = \Gamma_{\text{tot}}(\psi) - (R_{\text{had}}+2)\Gamma_{ee}(\psi) - \Gamma_{\gamma gg}(\psi)$$

$$= 44 \text{ keV}, \qquad (2.21)$$

$$\alpha_s(\psi) = \tfrac{3}{4}\kappa = 0.39. \qquad (2.22)$$

In (2.21) we have used the analogs of (2.19) and (2.20), and $R_{\text{had}} = 2.5$. This value of $\alpha_s(\psi)$, which is associated with our choice of $\kappa = 0.52$, is close to the value of α_s deduced from analyses of lepton production,[31] but it is about a factor of 2 larger than that determined from the naive formulas for $\Gamma_{ee}(\psi)$ and $\Gamma_{3g}(\psi)$. Part of the discrepancy may be due to unusually large higher-order radiative corrections to these results. The running coupling constant $\alpha_s(\Upsilon)$ is computed from the renormalization group equation

$$\alpha_s(\Upsilon) = \frac{\alpha_s(\psi)}{1 + [\alpha_s(\psi)/12\pi](33 - 2N)\ln(M_\Upsilon^2/M_\psi^2)}, \qquad (2.23)$$

with $N = 4$, the number of flavors. Finally, hadronic transitions are estimated by the multipole expansion of QCD.[32] For example,

$$\frac{\Gamma(\Upsilon' \to \pi\pi\Upsilon)}{\Gamma(\psi' \to \pi\pi\psi)} \cong \frac{\langle r^2 \rangle_\Upsilon^2}{\langle r^2 \rangle_\psi^2}. \qquad (2.24)$$

Results of these estimates are summarized in Table VI, and culminate in a width

$$\Gamma_{\text{tot}}(\Upsilon) = 21 \text{ keV}. \qquad (2.25)$$

This is below the present experimental limit[20]

$$\Gamma_{\text{tot}}(\Upsilon) > 25 \text{ keV (95\% C.L.)}. \qquad (2.26)$$

So far we have assumed the same potential for both the ψ and Υ families. To indicate the sensitivity of the results to the choice of parameters we have also performed a calculation by letting κ vary according to (2.23) which, for $\kappa(\psi) = 0.52$, gives

$$\kappa(\Upsilon) = 0.33. \qquad (2.27)$$

Keeping m_b and a as before, but changing α_s to $\tfrac{3}{4}\kappa(\Upsilon)$ in (2.2), we find that

TABLE VI. Estimated decay rates of $b\bar{b}$ states (keV). For the method of estimating various rates, see discussion in text.

State	Gluon annihilation	$\Gamma_{``\gamma''}$ [a]	$\Gamma_{\gamma gg}$ [b]	Photon transition [c]	Hadronic transition	Total width
$\Upsilon(9.46)$	12	8.7	0.3	~0		21
$\Upsilon'(10.01)$	4.3	3.2	0.1	2.5	≈ 7.8	≈ 18
$\Upsilon''(10.40)$	3.0	2.2	0.1	5.6	?	≥ 11
$1P_{J=2}(9.91)$	~220			36		260
$1P_{J=1}(9.91)$	~93			36		130
$1P_{J=0}(9.91)$	~660			36		700

[a] $\Gamma_{``\gamma''}$ is the decay rate via a virtual photon by the second-order electromagnetic interaction, including lepton pairs and hadrons. We have used (2.20) with $R_{\text{had}} \simeq 4$ at $W \simeq 10$ GeV.

[b] $\Gamma_{\gamma gg}$ is the rate for the inclusive decay into a single photon plus light hadrons.

[c] Rate of $E1$ transitions taken from Table V.

$$\Gamma_{e^+e^-}(\Upsilon) = 0.9 \text{ keV},$$

$$\Gamma_{e^+e^-}(\Upsilon') = 0.46 \text{ keV},$$ (2.28)

which are not far off the data [cf. Eq. (2.16)]. But the spectrum is markedly modified. For example,

$$m(\Upsilon') - m(\Upsilon) = 454 \text{ MeV}$$ (2.29)

instead of 592 MeV for $\kappa = 0.52$. This value (2.29) is very close to the value ~430 MeV that follows from the parameter set B given by (2.5). Equation (2.29) suggests that a value of κ fixed at 0.52 is favored by the (meager) data presently available about the Υ family. This is another indication that κ is not simply related to the running coupling constant in QCD.

To conclude this section, we have plotted in Fig. 4 the low-lying spectrum of heavier $Q\bar{Q}$ systems predicted by our potential with the parameter set A ($\kappa = 0.52$ fixed) as a function of the quark mass m_Q.

III. OUTLINE OF THE COUPLED-CHANNEL MODEL

When the total energy W exceeds the charm threshold, at 3.726 GeV, $c\bar{c}$ states can undergo OZI-allowed decays into charmed mesons. At that point the naive model has broken down. There is nothing novel about this; indeed, what is novel in the "new" spectroscopy is that there are $Q\bar{Q}$ states that are essentially bound, and where decay is not a prominent feature. In the quark model
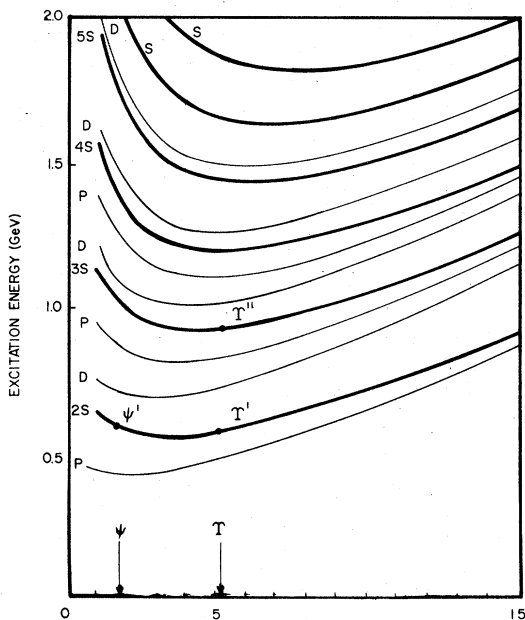
FIG. 4. Excitation energies for $Q\bar{Q}$ bound states as functions of the heavy quark mass m_Q. The model and its parameters are given in Eqs. (2.1) and (2.4).
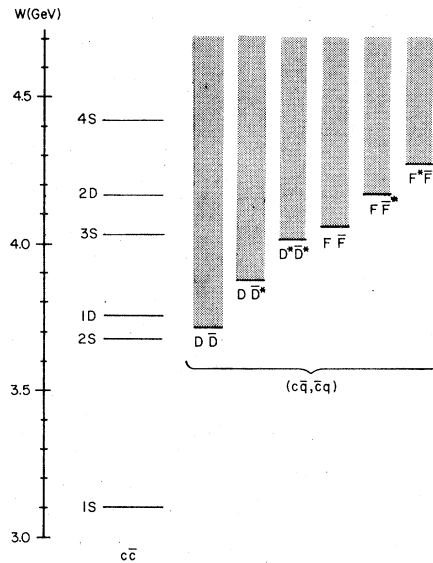
FIG. 5. The spectra of the $c\bar{c}$ system, and of the lowest-lying charmed-meson decay channels.

work on the "old" spectroscopy surprisingly little attention[33] was devoted to decay phenomena even though they are pervasive there. Encouraged by the greater simplicity of heavy-quark phenomena, we have attempted to incorporate OZI-allowed decay phenomena into the model. The mathematical details of how this is done were already described in Sec. III of I, and will not be repeated. Nevertheless, for the benefit of more casual readers we shall outline the ideas that underlie this formalism here.

The problem we face is most aptly summarized by Fig. 5, which shows the observed resonances that we ascribe to $c\bar{c}$ states, and the spectra of the known quasi-two-body charmed meson states in the vicinity of the charm threshold. This is a classic problem of quantum mechanics: a discrete set of states in one portion of the Hilbert space suspended in a continuum of states belonging to another subspace.

A. Extension of the model to incorporate OZI-allowed decays

To make contact with reality we must introduce an interaction that allows communcation between the $c\bar{c}$ and $(c\bar{q}, \bar{c}q)$ states of Fig. 5. A realistic description of such interactions, rooted in the foundations of QCD, is not yet in sight. In view of this we have generalized the naive $c\bar{c}$ model in the simplest way imaginable. That is, we write the interaction of the naive model in second quantized form:

$$H_i = \frac{3}{8} \sum_{a=1}^{8} \int \, :\rho_a(\vec{r})V(\vec{r}-\vec{r}')\rho_a(\vec{r}'): d^3r\, d^3r' \, ,$$

(3.1)
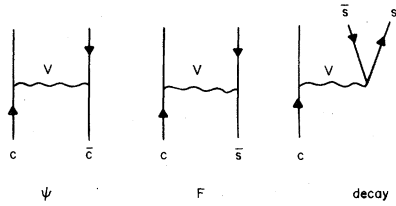
FIG. 6. Some interactions contained in Eq. (3.1).

where V is the potential that appears in the Schrö-dinger equation of the naive $c\bar{c}$ model, and $\rho_a(\vec{r})$ $\equiv \frac{1}{2}\psi^{\dagger}(\vec{r})\lambda_a\psi(\vec{r})$ is the octet of color densities, with ψ being the quark field operator. In the $c\bar{c}$ sub-space, (3.1) reduces to the model of Sec. II. But when ψ is decomposed into creation and destruction operators, a variety of other terms appear. Among these are the processes depicted in Fig. 6. Here we see $c\bar{c}$ and $c\bar{s}$ interactions that lead to the bound states ψ and F, respectively, but we also see a pair-creation term $c \rightarrow cs\bar{s}$, and this con-nects the two- and four-quark subspaces of Fig. 5. This last amplitude in Fig. 6, and the one for the inverse process, are responsible for the OZI-allowed decays, and are fully incorporated in the calculations to be described. [The interaction (3.1) also has terms not shown in Fig. 6 (see Fig. 5 of I), but which are ignored on a variety of grounds; see Sec. III D of I.]

We can now use H_I to evaluate an OZI-allowed decay amplitude, say the matrix element

$$\langle c\bar{c}, n^{2S+1}L_J | U | c\bar{s}, \alpha; \bar{c}s, \bar{\beta}; \vec{p} \rangle,$$

where the bra is a $c\bar{c}$ state with the indicated quantum numbers, and the ket contains a charmed-strange meson pair with spin-parities α and $\bar{\beta}$, and relative momentum $2\vec{p}$. The operator U is re-lated to (3.1) by $U = P_\psi H_I P_C$, where P_ψ and P_C are projection operators onto the $c\bar{c}$ and $c\bar{q}, \bar{c}q$ sub-spaces. Such a matrix element for $\bar{F}F^*$ decay is illustrated in Fig. 7. Its actual form, apart from
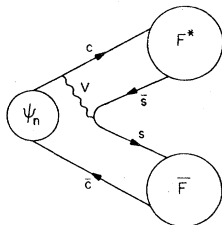
FIG. 7. The amplitude for $\psi_n(c\bar{c}) \rightarrow \bar{F}F^*$. Observe that it can be viewed as a combination of the elementary amplitudes that appear in Fig. 6, with the "binding" ex-changes incorporated into the wave functions, here designated by circles. The complete amplitude is a sum of two terms, the one shown, and another where V attaches to the $\bar{c}$ line.

a trivial factor C is

$$\langle c\bar{c} | U | \bar{F}F^*; \vec{p} \rangle$$

$$= \frac{C}{m_s} \int d^3x\, d^3z\, (\chi_s^{\dagger} \vec{\sigma} \cdot \hat{x} \chi_{\bar{s}})$$

$$\times \frac{dV(x)}{dx}\, \phi_F^*(\vec{x})\phi_{F^*}^*(\vec{x} - \vec{y})\psi_n(\vec{y})e^{-i\mu\vec{p}\cdot\vec{y}},$$

(3.2)

where $\mu = m_c/(m_c + m_s)$. Here ψ_n is the $c\bar{c}$ wave function, and the ϕ's are the wave functions of the decay products; all three functions pertain to the same potential V. Equation (3.2) results after a nonrelativistic reduction, and $\chi^{\dagger}$ and χ are there-fore Pauli spinors. The pseudoscalar $\vec{\sigma} \cdot \hat{x}$ appears because a static potential creates a pair in the ^1S state. In our numerical calculations we have, for simplicity, ignored all effects of the Coulomb term of the potential both in (3.1) and in the wave functions, and approximated the wave functions of the ground-state charmed mesons by Gaussians.

Obviously (3.2) represents a very simplistic ap-proximation to a hadronic decay amplitude. Never-theless, it incorporates the crucial feature that the parent and its decay products are all extended systems. For example, the fact that $Q\bar{Q}$ states are much smaller than $Q\bar{q}$ states when $m_Q \gg m_q$ is taken into account. This is an aspect of the new spectroscopy that seems to be unprecedented in physics; we are not accustomed to systems that decay into objects considerably larger than them-selves.

As we saw in I (see Figs. 9 and 10), the decay amplitudes (3.2) are oscillatory functions of $|\vec{p}|$: There is a close correlation between the number of radial nodes in $\psi_n(r)$ and the number of zeros of (3.2).

B. Dynamics of coupling between $c\bar{c}$ states and charmed mesons

Equation (3.2) provides Born amplitudes for OZI-allowed decays. If the associated rates were small (i.e., widths negligible compared to the $c\bar{c}$ level spacing) we could use Fermi's "golden rule," and that would be the end of the matter. But above the charm threshold these rates are large, and one must treat the decay more seriously.

Our first task is to find a suitable object from which to compute the quantities that interest us. To motivate the definition of this object, we recall the Green's function associated with a conventional Schrödinger problem with Hamiltonian H_0:

$$G(\vec{r}, \vec{r}'; z) \equiv \langle \vec{r} | (z - H_0)^{-1} | \vec{r}' \rangle \qquad (3.3)$$

$$= \sum_n \frac{\psi_n(\vec{r})\psi_n^*(\vec{r}')}{z - E_n} + \int_0^{\infty} dE\, \frac{\psi_E(\vec{r})\psi_E^*(\vec{r}')}{z - E},$$

(3.4)

where ψ_n and ψ_E are eigenfunctions in the discrete and continuous spectra, respectively, and z is a complex variable. If we wish to know the probability of finding a particle at the origin and having an energy E in the continuous spectrum, we can determine it from (3.4) via

$$|\psi_E(0)|^2 = -(1/\pi)\text{Im}G(0,0;E+i\epsilon) . \qquad (3.5)$$

Thus if our $c\bar{c}$ pair were interacting through a potential that does *not* confine, (3.5) would provide the way for computing $e^+e^- \to c\bar{c}$ above the threshold for free quark production.

The true situation is actually not totally unrelated to this unrealistic model. The coupling to the $(c\bar{q}, \bar{c}q)$ states does allow c and $\bar{c}$ to escape to infinity, provided each of them is accompanied by another quark, and this escape mechanism can be represented by an effective interaction Hamiltonian that acts *only* in the $c\bar{c}$ sector. One might jump to the conclusion that this is an idiotic approximation, but the opposite is true: In *any* problem with N degrees of freedom one can always confine one's attention to a subset of $n < N$ degrees of freedom by constructing an effective interaction Ω that will describe the evolution of this subset *exactly*. Naturally Ω is, in general, a very complicated operator—in particular, it will not be Hermitian if "decay" can occur.

Assume that we already know this Ω for our $c\bar{c}$ subspace; it will, as we have said, implicitly contain all information about the coupling between the $c\bar{c}$ states and others that have more quarks. With this Ω we construct the "true" Green's function $\mathcal{G}(\vec{r},\vec{r}';z)$ in the $c\bar{c}$ subspace using the universal definition (3.3) by simply replacing H_0 by $H_0 + \Omega$. The contribution to $\sigma(e^+e^- \to \text{hadrons})$ stemming from $c\bar{c}$ creation is then computed in the usual manner by combining (3.5) with the van Royen–Weisskopf formula. As we showed in Appendix C of I, this calculation yields the following formula for the cross section due to charmed final states, divided by $\sigma(e^+e^- \to \mu^+\mu^-)$:

$$\Delta R = -(32\pi/W^2)\text{Im}\mathcal{G}(0,0;W+i\epsilon) . \qquad (3.6)$$

The isolated poles of $\mathcal{G}$ also give us the new position of the bound states, i.e., the shifts due to coupling to closed decay channels, and their residues the components of the bound-state eigenvectors in the $c\bar{c}$ sector. This makes it clear that when one incorporates decay, one must "renormalize" the parameters of the naive model (quark masses, parameters in V) so that the *final* spectrum of bound states and thresholds is as in Fig. 5.

Thus a knowledge of the effective $c\bar{c}$ interaction due to open and closed decay channels is all that is needed to compute the quantities of interest to us. In I (see Sec. III E) we showed that the amplitudes depicted in Fig. 7 lead to the following expression for Ω:

$$\Omega_{nm}(W) = \sum_\tau \int d^3p_1 d^3p_2 \frac{\langle n|U|\tau\vec{p}_1\vec{p}_2\rangle\langle\tau\vec{p}_1\vec{p}_2|U^\dagger|m\rangle}{W-E_1-E_2+i\epsilon} .$$

$$(3.7)$$

Here the matrix elements are just the expressions (3.2), i.e., τ is a channel index (e.g., $\bar{D}D^*$), $(E_i, \vec{p}_i)$ are the four-momenta of the decay products, and $|n\rangle$ and $|m\rangle$ are *any* pair of $c\bar{c}$ states sharing the same conserved quantum numbers (e.g., 1^3D_1 and 2^2S). Observe that Ω is indeed a complex matrix once W exceeds the $D\bar{D}$ threshold.

We quickly list the approximations made in arriving at (3.7): Only valence quarks are retained—matrix elements of U that produce sea quarks are discarded; the fact that the decay products may themselves be unstable (i.e., $D^* \to D\pi$) is ignored, as are OZI-forbidden decays; final-state interactions are neglected; all expressions are reduced to their nonrelativistic limit. Of these the last is probably the most serious. While the c quarks move fairly slowly, and make a nonrelativistic description of the $c\bar{c}$ bound states a reasonable first approximation, there is no justification for treating the light quarks in this way. These calculations are therefore based on the hope that a more realistic calculation would have qualitatively similar decay amplitudes.

The Green's function $\mathcal{G}$ constructed with this Ω describes the propagation of a $c\bar{c}$ pair in a manner that incorporates all real or virtual decays into noninteracting charmed-meson pairs, and may therefore be depicted by Fig. 8; $\mathcal{G}$ contains *all* diagrams of this type.

So far we have only discussed the approximations inherent to the very scheme that culminates in the formulas for the decay amplitudes and the effective interaction Ω. This is the straightforward part of the story. Unfortunately it is not practical to evaluate Ω for a complete set of decay channels $|\tau\rangle$ as well as $c\bar{c}$ states $|n\rangle$. The calculations done thus far actually involve two important truncations. The first of these is that we only keep the first few $c\bar{c}$ bound states $|n\rangle$, and thereby reduce Ω to a finite matrix. This approximation is easily controlled by straightforwardly adding further states and examining the stability of the final result. The
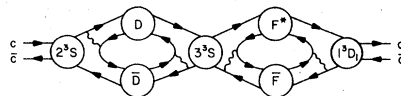
FIG. 8. The propagation of a $c\bar{c}$ pair in the presence of open and closed decay channels as described in the Green's function $\mathcal{G}$.

second truncation is far more drastic: Only ground-state charmed mesons are retained, i.e., the channels shown in Fig. 5. It is therefore obvious that the present calculations are only meaningful below $W \lesssim 4.3$ GeV, where production of p-wave charmed mesons is expected to become significant. (This expectations appears to be borne out by SPEAR results[34] indicating that by $W = 4.415$ GeV there may be copious production of objects having a mass of ~2.44 GeV and decaying into $D^*\pi$.)

The restriction to such a small set of decay channels represents a very severe handicap. On the practical side, it means that our calculations, though very laborious and complex, do not reach many of the interesting structures observed in R. Furthermore, the computed positions of resonances stemming from primordial $c\bar{c}$ bound states that lie near the truncation point are merely artifacts of the approximation. The austere simplicity of the original scheme, where all parameters are contained in the one universal interaction (3.1), is therefore marred. In particular, one must lower the positions of resonances near the brink (in practice, of 3^3S) by hand to mock-up the depression that would ensue if final states containing excited D's and F's were included in Ω. On the more theoretical side, the truncation leaves unanswered the serious question of whether Ω exists [i.e., whether (3.7) needs a subtraction].

Despite this long list of shortcomings, one should not lose sight of the fact that this extension of the model to the above-threshold region represents a significant first step beyond the naive quark model.

IV. THE INFLUENCE OF CLOSED DECAY CHANNELS ON $c\bar{c}$ BOUND STATES

A. Determination of model parameters

Our calculation of the charmonium system based on the coupled-channel method developed in I, and outlined in Sec. III, proceeds as follows.

(a) We assume initial values for m_c and a, calculate the decay amplitudes (3.2), and the elements of the matrix Ω by use of (3.7). Following the discussion of Sec. III, we only include production of $D\bar{D}$, $D^*\bar{D}$, $D^*\bar{D}^*$, $F\bar{F}$, $F^*\bar{F}$, $F^*\bar{F}^*$ in calculating Ω_{nm}, and truncate the matrix Ω by restricting the number of ^3S and ^3D states of the $c\bar{c}$ system to be included. The following parameters are fixed throughout our calculation[35]:

$$m_u = m_d = 0.335, \quad m_s = 0.450,$$
$$m(D^0) = 1.863, \quad m(D^{*0}) = 2.006,$$
$$m(D^+) = 1.868, \quad m(D^{*+}) = 2.008, \quad \text{(4.1a)}$$
$$m(F) = 2.040, \quad m(F^*) = 2.140,$$

(all in GeV) and

$$\kappa = 0.517, \quad (\alpha_S = \tfrac{3}{4}\kappa). \quad \text{(4.1b)}$$

(b) We solve the eigenvalue problem

$$\text{Det}\,|(z - \epsilon_n)\delta_{nm} - \Omega_{nm}(z)| = 0, \quad \text{(4.2)}$$

where ϵ_n are eigenvalues of the naive model of Sec. II, and find the eigenvalues of the coupled system. For $\text{Re}\,z < W_c$, where $W_c = 2m_D$ is the charm threshold, the zeros of (4.2) lie on the real axis and locate the bound-state energies. The additive constant in the potential is adjusted so that the first zero of (4.2) coincides with the mass of ψ. The distance between the lowest two eigenvalues corresponds to $m(\psi') - m(\psi)$. The residue of $\mathcal{G}$ at the lowest eigenvalue is related to the leptonic width $\Gamma_{e^+e^-}$ of ψ. In general these values do not agree with the observed values which are

$$m(\psi') - m(\psi) = 0.589 \text{ GeV}, \quad \text{(4.3)}$$

$$\Gamma_{e^+e^-}^{\text{theory}}\left(1 - \frac{4\kappa}{\pi}\right) = 4.8 \text{ keV}. \quad \text{(4.4)}$$

The correction factor $(1 - 4\kappa/\pi)$ was discussed in detail in Sec. II A.

(c) We choose new values of m_c and a and repeat the steps (a) and (b) until the calculated values of $m(\psi') - m(\psi)$ and $\Gamma_{e^+e^-}^{\text{theory}}$ agree with (4.3) and (4.4).

(d) We enlarge the size of the truncated Ω matrix to include more $c\bar{c}$ states and repeat the steps (a)–(c). (The region below ~4.3 GeV becomes fairly stable when four S states and two D states are included.)

Proceeding in the manner described above, we have arrived at

$$m_c = 1.84 \text{ GeV},$$
$$a = 2.12 \text{ GeV}^{-1} \quad \text{(4.5)}$$

as our preferred choice. On comparing with the naive values of (2.4), we see that m_c is not changed significantly.

B. Energy spectrum, eigenstates, and radiative transition rates

Despite the fact that our basic interaction is spin independent, the hyperfine splittings between D^* and D, and F^* and F, induce spin-dependent forces in our coupled-channel calculation. In particular, it will cause S-D mixing and splitting of the P states.

The "bare" masses of the n^3S_1 and n^3D_1 states corresponding to these values of m_c and a, the mass shift due to coupling to decay channels, and the "renormalized" masses are listed in Table VII. That the mass shift of 2^3S_1 is much larger than that of 1^3S_1 is a reflection of the closeness of the ψ' state to the $D\bar{D}$ threshold. The rather small

TABLE VII. Mass shifts in the coupled-channel cal-
culation of charmonium states; see the text for the pa-
rameters used.

State	Bare mass (MeV)	Mass shift (MeV)	Renormalized mass (MeV)
1^3S_1	3143	−48	3095
2^3S_1	3802	−118	3684
3^3S_1	4280	−55	4225
4^3S_1	4687	−62	4625
1^3P_2	3615	−92	3523
1^3P_1	3615	−98	3517
1^1P_0	3615	−96	3519
1^3D_1	3935	−180	3755
2^3D_1	4372	−142	4230

shifts of 3S and 4S are presumably due to the
omission of additional thresholds involving orbital
and radial excitations of charmed mesons. Also
the masses of 3S and 2D are difficult to determine
because of large interference effects in this re-
gion.

The wave functions for the "physical" ψ and ψ'
are now linear combinations of various bare
states. For example, the structure of ψ' is of the
form

$$|\psi'\rangle = \sum_n a_n |n^3S(c\bar c)\rangle + \sum_n b_n |n^3D_1(c\bar c)\rangle$$
$$+ \alpha|D\bar D;p\text{-wave}\rangle + \beta|D^*\bar D^*;f\text{-wave}\rangle + \cdots,$$

$$(4.6)$$

where a_2 is the largest coefficient. Although the
states in the second line have the spatial structure
of bound states of charmed mesons, these are *not*
"molecular" states[36] because ψ' lies below the
threshold. The amount of mixing in ψ and ψ' from

other S and D states is listed in Table VIII. The
effect of mixing with virtual charmed-meson states
is also listed in the column entitled $Z_{(c\bar c)}$. The
departure from unity, $1 - Z_{(c\bar c)}$, is the probability
of finding the state in the charmed-meson sector.

As a consequence of mixing, the ratio of the
wave functions for ψ' and ψ at the origin squared
is changed to 0.67 from that given by (2.6). The
resulting leptonic width of ψ' is in complete agree-
ment with experiment (see Table VIII).

Using the parameters (4.5) determined above,
one can also find the positions of the P states by
a similar calculation. The bare masses, mass
shifts, and renormalized masses for 1P states
are shown in Table VII. The center of gravity of
the 1P states is 3.521 GeV to be compared with
the observed value 3.522 GeV.

The splitting of these levels due to the coupled-
channel effect (induced splitting) is only a few
MeV, and is far too small to account for the ob-
served splitting. Clearly the major part of the
1P state splitting must come from the sizeable
spin-orbit force which is expected to be present
in any system bound together by vector-meson ex-
change.

The amount of mixing of other P states in 1^3P_J
is also listed in Table VIII.

Given the wave functions listed in Table VIII,
we can evaluate the E1 matrix elements, including
the effects of coupling to virtual decay channels,
using Eqs. (2.21), (3.53), and (3.55) of I and other
formulas given in Appendices D, E, and F of I.
We find that, although the $D\bar D^* + D^*\bar D$ thresholds
are more distant from ψ', their effects are as
important as the $D\bar D$ threshold because statistical-
ly they are much stronger thresholds. Calculated
results for the E1 transitions $\psi' \to \gamma\chi_J$ and $\chi_J \to \gamma\psi$
are shown in Tables IX and X, respectively.

TABLE VIII. Modification of $c\bar c$ states due to decay. The probability amplitude for a phys-
ical particle (ψ, ψ', or χ_J) to be in a charmonium state is given by the number under that
state. $Z_{(c\bar c)}$ gives the norm of the physical particle in the $c\bar c$ sector. [a] $\Gamma_{ee}(\psi)$ is held fixed at
4.8 keV.

Particle	1S	2S	3S	4S	1D	2D	$Z_{(c\bar c)}$	Γ_{ee} (keV)
ψ	0.982	0.040	−0.010	0.003	-2×10^{-4}	-7×10^{-6}	0.966	4.8
ψ'	−0.090	0.883	0.046	−0.015	−0.031	0.006	0.791	2.3

Particle	1P	2P	3P	$Z_{(c\bar c)}$
χ_2	0.938	−0.063	−0.014	0.885
χ_1	0.933	−0.060	−0.014	0.874
χ_0	0.937	−0.055	−0.013	0.881

[a] For this and the remaining tables the bare masses of 1^3P_J states have been shifted so that
the renormalized masses are 3.415, 3.510, and 3.555 GeV for the J=0, 1, and 2 states, re-
spectively. These shifts are −107, −8, and 36 MeV, respectively, for J=0, 1, and 2 1^3P_J
states.

TABLE IX. $E1$ transitions $\psi' \to \chi_J + \gamma$ by coupled-channel calculation. [a,b]

	$J=0$	$J=1$	$J=2$
j^ψ	1.245 [c]	1.283 [c]	1.298 [c]
j^c	0.297	0.256	0.264
j^X	−0.044	−0.017	−0.048
$Z(2S)Z(1P_J)\|\langle 2S\|D\|1P\rangle\|^2$	1.537	1.572	1.571
J_{SP}	−0.014	−0.014	−0.027
J_{SD}	0.180	−0.091	0.019
$\|\epsilon_{if}\|^2$	1.703	1.494	1.617
Rate (keV)	43.2	34.4	23.7
Rate/naive rate [d]	0.86	0.76	0.82

[a] See footnote a in Table VIII.

[b] The notation in this table is explained in Sec. IV.

[c] Dependence on the photon momentum is included in the calculation of matrix elements. Hence the results are slightly different for states of different J.

[d] These are the ratios of the rates to those in Table I.

To explain the notations used in these tables, we outline briefly our calculational procedure. For our numerical calculation we write the $E1$ transition rate as

$$\Gamma_{E1} = \frac{4}{9} e_c^2 \alpha k^3 |\epsilon_{if}|^2 (2J_f + 1) , \qquad (4.7)$$

where k is the photon momentum. In terms of the expansion coefficients of a charmonium state $|\alpha JM\rangle$ in the $c\bar{c}$ sector,

$$P_\psi |\alpha JM\rangle = \sum_{nL} a_{nL}^{\alpha J} |\psi; nLJM\rangle , \qquad (4.8)$$

ϵ_{if} can be expressed in the form

$$\epsilon_{if} = \sum_{nL,n'L'} a_{nL}^{i\ *} a_{n'L'}^{f} \cdot (j_{nL,n'L'}^\psi + j_{nL,n'L'}^C + j_{nL,n'L'}^X) . \qquad (4.9)$$

Here $j_{nL,n'L'}^\psi$, $j_{nL,n'L'}^C$, and $j_{nL,n'L'}^X$ are the transition electric dipole matrix elements in the $c\bar{c}$ sector, the charm sector, and due to pair creation

TABLE X. $E1$ transitions $\chi_J \to \psi + \gamma$ by coupled-channel calculation. [a]

	$J=0$	$J=1$	$J=2$
j^ψ	1.000	0.979	0.966
j^c	0.108	0.112	0.112
j^X	−0.026	−0.018	−0.019
$Z(1P_J)Z(1S)\|\langle 1P\|D\|1S\rangle\|^2$	0.992	0.966	0.953
J_{SP}	0.076	0.068	0.063
J_{SD}	0.001	−0.0004	0.0001
$\|\epsilon_{if}\|^2$	1.069	1.033	1.017
Rate (keV)	130	257	350
Rate/naive rate	0.92	0.89	0.88

[a] See footnotes a, b, c, and d in Table IX.

linking the $c\bar{c}$ sector and charm sector, respectively. The precise definitions of these quantities are contained in Appendices E and F of I. Using (4.6) and a similar expansion for the χ_J states,

$$|\chi_J\rangle = \sum_n c_n^J |n^3P_J(c\bar{c})\rangle + \gamma|D\bar{D}\rangle + \cdots , \qquad (4.10)$$

we have for the transition $\psi' \to \gamma + \chi_J$

$$|\epsilon_{if}|^2 = Z(2S)Z(1P_J)|\langle 2S|D|1P\rangle|^2 + J_{SP} + J_{SD} + \cdots , \qquad (4.11)$$

where

$$Z(2S) = |a_2|^2 ,$$
$$Z(1P_J) = |c_1^J|^2 , \qquad (4.12)$$

$$\langle 2S|D|1P\rangle = j^\psi + j^C + j^X \quad (j^\psi \equiv j_{20,11}^\psi, \text{ etc.}), \qquad (4.13)$$

$$J_{SP} = \sum_{\substack{n,n'=1,2,3 \cdots \\ m,m'=1,2,3,\cdots}} a_n^* a_{n'} c_m^J c_m^{J\ *} D_{n'0,m'1}^* D_{n0,m1}$$

$$(n=n'=2, \ m=m'=1, \text{ excluded}), \qquad (4.14)$$

$$J_{SD} = \sum_{n=1,2,3} \sum_{n'=1,2} a_n^* b_{n'} Z(1P_J) D_{n0,11} D_{n'2,11}^* + \text{c.c.} , \qquad (4.15)$$

$$D_{nL,n'L'} \equiv j_{nL,n'L'}^\psi + j_{nL,n'L'}^C + j_{nL,n'L'}^X . \qquad (4.16)$$

J_{SP} arises from mixing of $2S$ and $1P$ with other S and P states while J_{SD} is due to S-D mixing. In our numerical calculation only $j_{nL,n'L'}^\psi$ is kept in J_{SP} and J_{SD}, j^X and j^C being much smaller. Other terms not explicitly included in (4.11) are very small and neglected.

For the transitions $\chi_J \to \psi + \gamma$ analogous quantities can be defined by equations similar to (4.9)–(4.16) with the roles of $1S$ and $2S$ interchanged.

From the tables we note that the charmed-meson sector makes a significant contribution to $E1$ transitions while the contribution of the pair term j^X is rather small. The final results for the $E1$ rates are significantly reduced from the corresponding rates in the naive model. However, they are still larger than the data by about a factor of 2. Ex-

TABLE XI. Comparison of radiative transitions by naive-model and coupled-channel calculation and experiments.

Transition	Naive model (keV)	Coupled channel (keV)	Experiment (keV)
$\psi' \to \chi_0 + \gamma$	50	43.2	16 ± 9
$\psi' \to \chi_1 + \gamma$	45	34	16 ± 8
$\psi' \to \chi_2 + \gamma$	29	23.7	16 ± 9

perimental values, naive-model values, and the coupled-channel results are compared in Table XI.

V. e^+e^- ANNIHILATION ABOVE THE CHARM THRESHOLD

Our calculation of the charmed component ΔR of R is based on two assumptions: (1) Production of charm is mediated by those chamonium states which couple to the photon; (2) the basic production process is quasi-two-body, i.e., of the form $e^+e^- \rightarrow D_1\overline{D}_2$ (and $F_1\overline{F}_2$) where D_1 is a $c\bar{u}$ or $c\bar{d}$ meson.[37] The first assumption is just vector-meson dominance, taking into account the mixing of $J^{PC} = 1^{--}$ $c\bar{c}$ states through their coupling to decay channels. Obviously, we can expect this approximation to be useful only in the "resonance region," $W \lesssim 4.3$ GeV.[38] Quasi-two-body production is well motivated by past experience in hadronic processes. When valid it has the important consequence that at a fixed energy W the distribution

of invariant mass recoiling against D's or F's is a useful tool in unraveling the charmed-meson spectrum.

A. Qualitative discussion of exclusive-channel ratios in e^+e^- annihilation

To understand the structure of our computed ΔR, and to gain insight into the actual data, it is helpful to discuss in some detail our formula for ΔR. (This discussion expands somewhat on remarks made in Secs. III F and III G of I.) The formula for ΔR is a sum over exclusive-channel ratios,

$$\Delta R(W) = \sum_i R_i(W), \tag{5.1}$$

where i runs over the two-body channels. The explicit form for the production of strangeness-zero charmed mesons is

$$
\begin{bmatrix} R_1 \\ R_2 \\ R_3 \end{bmatrix} = \frac{32\pi^2}{W^3} p_i E_1 E_2 f_u^2 \sum_{m,n} \sum_{m',n'} \psi_{m0}(0) \left\{ \mathcal{G}^*_{m0,n0} \begin{bmatrix} \frac{1}{3} \\ \frac{4}{3} \\ \frac{7}{3} \end{bmatrix} I^1_{n0}(p_i) I^1_{n'0}(p_i) \mathcal{G}_{n'0,m'0} \right.
$$

$$
+ \mathcal{G}^*_{m0,n2} \begin{bmatrix} -\sqrt{2}/3 \\ 2\sqrt{2}/3 \\ -\sqrt{2}/3 \end{bmatrix} I^1_{n2}(p_i) I^1_{n'0}(p_i) \mathcal{G}_{n'0,m'0} + \text{c.c.}
$$

$$
\left. + \mathcal{G}^*_{m0,n2} \left[\begin{bmatrix} \frac{2}{3} \\ \frac{2}{3} \\ \frac{4}{15} \end{bmatrix} I^1_{n2}(p_i) I^1_{n'2}(p_i) + \begin{bmatrix} 0 \\ 0 \\ \frac{12}{5} \end{bmatrix} I^3_{n2}(p_i) I^3_{n'2}(p_i) \right] \mathcal{G}_{n'2,m'0} \right\} \psi_{m'0}(0)
$$

$$
\text{for } i = \begin{cases} 1: & D\overline{D} \\ 2: & D\overline{D}^* + D^*\overline{D} \\ 3: & D^*\overline{D}^* \end{cases} \tag{5.2}
$$

Here, p_i is the momentum of either meson in the ith channel, E_1, E_2 the energy of $D_1, \overline{D}_2$, and $E_1 + E_2 = W$. An analogous but simpler formula holds for F-meson production. We turn now to a detailed discussion of (5.2).

The constant f_u^2 was given in Eq. (3.42) of I[39]:

$$
f_q^2 = \tfrac{2}{3}(m_q \alpha^2 \beta^{3/2}\pi)^{-2} = \frac{3}{\pi}\left(m_q \frac{m_c m_q}{m_c + m_q}\right)^{-2}; \quad q = u, d, s. \tag{5.3}
$$

As discussed in I, the first factor, the light-quark mass m_q, arises from the production mechanism of the light $q\bar{q}$ pair in the transition $\psi_{nL}(c\bar{c}) \rightarrow D_1(c\bar{q}) + D_2(\bar{c}q)$; it is a consequence of the nonrelativistic

approximation to the Hamiltonian H_I in Eq. (3.1). The reduced mass comes from $c\bar{q}$ and $\bar{c}q$ bound-state wave functions. Together, these factors imply a substantial suppression of F production relative to D. Neglecting other less important dependences on m_q, we expect (for large enough W) that

$$
\sigma(e^+e^- \rightarrow F^+ + \dots) \sim \left(\frac{m_u}{m_s}\right)^4 \sigma(e^+e^- \rightarrow D^+ + \dots)
$$

$$
\sim \frac{1}{2}\left(\frac{m_u}{m_s}\right)^4 [\sigma(e^+e^- \rightarrow D^+ + \dots)
$$

$$
+ \sigma(e^+e^- \rightarrow D^0 + \dots)]. \tag{5.4}
$$

With $m_u \simeq 0.33$ GeV, $m_s \simeq 0.45$ GeV, inclusive F production is 20–30% of *either* inclusive D^+ or D^0 production at most energies between F threshold and $W \sim 6$–7 GeV (where one might reasonably expect asymptotic behavior to set in). Deviations from this rule may arise from momentum dependence of the "form factors" $I_{nL}^l(p)$ (see below).

The sum in R_i runs over the radial quantum numbers of the 1^{--} charmonium states. In the nonrelativistic approximation their coupling to the photon is controlled by the wave function $\psi_{mL}(0)$ at zero $c\bar{c}$ separation, so only $^3S_1$ states contribute. Thus, $\psi_{m0}(0)$ projects out only those parts of the resolvent $\mathcal{G}$ which link m^3S_1 to n^3S_1 ($\mathcal{G}_{m0,n0}$), and m^3S_1 to n^3D_1 ($\mathcal{G}_{m0,n2}$). The vector-meson resonances appear as poles in $\mathcal{G}$ at $W_N = M_N - i\Gamma_N/2$. States which are mostly n^3S_1 show up most strongly in $\mathcal{G}_{m0,n0}$, with $m = n, n \pm 1$. Those which are mainly n^3D_1 appear strongest in $\mathcal{G}_{m2,n2}$, which does *not* contribute to R_i. In this model, therefore, n^3D_1 appears as a resonance in e^+e^- annihilation only through its mixing with a nearby $^3S_1$ state, i.e., as a pole in $\mathcal{G}_{m0,n2}$ with $m = n+1$. The mechanism for S-D mixing will be discussed shortly.

The relative production rates of the different channels are controlled by the amplitudes I_{nL}^l. Because of their falloff with p, and the structure of the matrix $\mathcal{G}$, only a few terms in (5.2) are important at the peak of a resonance. The bilinear forms in (5.2) involving the I_{nL}^l are essentially the absorptive part of the matrix Ω, defined in Eqs. (3.22) and (3.23) of I. For example,

$$\text{Im}\,\Omega_{m0,n0}^i = -\frac{\pi p_i E_1 E_2}{W} f_q^2 \begin{pmatrix} \frac{1}{3} \\ \frac{4}{3} \\ \frac{7}{3} \end{pmatrix} I_{m0}^1(p_i) I_{n0}^1(p_i) \qquad (5.5)$$

and

$$\text{Im}\,\Omega_{m0,n2}^i = -\frac{\pi p_i E_1 E_2}{W} f_q^2 \begin{pmatrix} -\sqrt{2}/3 \\ 2\sqrt{2}/3 \\ -\sqrt{2}/3 \end{pmatrix} I_{m0}^1(p_i) I_{n2}^1(p_i). \qquad (5.6)$$

Statistical factors (such as $\frac{1}{3}$, $\frac{4}{3}$, $\frac{7}{3}$) weighting the relative contributions of the three channels are just the C coefficients defined in Eq. (D19) of I. This is the origin of the infamous 1:4:7 ratio[40,41] for $e^+e^- \to D\bar{D}:D\bar{D}^* + D^*\bar{D}:D^*\bar{D}^*$. However, this ratio rule is correct only if $M_D = M_{D^*}$ so that $p_D = p_{D^*}$ at all W. Then $I_{nL}^l(p)$ has the same value for all three channels, and the S-D mixing matrix elements $\mathcal{G}_{m0,n2}(W)$ connecting $^3S_1$ and $^3D_1$ states vanish identically. Of course, $m_D \neq m_{D^*}$ and the relevant $I_{nL}^l(p)$ have such dramatic momentum de-

pendence in the region of interest that rules based on statistical factors alone are practically useless.

In our model, the assumed mass difference between D and D^* is the *only* source of spin dependence, and this has two very important consequences. First, it is responsible for the S-D mixing just noted. As a corollary, S-D mixing is strongest in our model when a $^3D_1$ pole sits in the midst of a set of spin-split thresholds (e.g., at $W \simeq 3.8$ GeV), and weakest when it is far from such thresholds so that p_i is approximately the same for all channels i sharing the same pairs of principal and orbital quantum numbers. We expect that there must also be spin-dependent terms in the $c\bar{c}$ potential which induce S-D mixing. This point will be discussed in more detail later.

The second effect of the D^*-D mass difference is to introduce a very marked energy dependence into the relative production rates of the various exclusive channels, beyond what one expects from the statistical and phase-space factors alone. This comes from the momentum dependence of I_{nL}^l which, up to factors independent of meson momentum, is the amplitude for ψ_{nL} (mass W) to decay in the lth partial wave to a pair of ground-state (0^- or 1^-) mesons, $D_1\bar{D}_2$ or $F_1\bar{F}_2$, having momentum

$$p_i = \{[W^2 - (M_1 + M_2)^2][W^2 - (M_1 - M_2)^2]\}^{1/2}/2W.$$

The I_{nL}^l are shown in Figs. 9 and 10 for three $^3S_1$ and two $^3D_1$ states. The most striking features of these figures are the nodes, increasing in number with the radial quantum number, and the fairly rapid falloff at higher momenta. Both reflect the nodes and the finite extent of the $c\bar{c}$ radial wave function R_{nL} and—insofar as they are observable—support the notion of bound quark constituents. Indeed, the presence of zeros in I_{nL}^l has an enormous influence on the relative abundance of each exclusive channel in the 4-GeV region, since any $c\bar{c}$ resonance above the $D^*\bar{D}^*$ threshold is certainly a radial excitation, and the momentum p_i of any open channel lies just in the region where the form factors are most rapidly varying. Although the precise location of these zeros may be fairly model dependent, their presence certainly is not; very similar behavior has been found in simpler model calculations of $\psi_{nL} \to D_1\bar{D}_2$.[42]

At high momentum, $I_{nL}^l(p)$ falls off as $p^{-(4+L)}$. Deduced from Eq. (3.37) of I, this power law certainly depends on our specific production mechanism and on the use of nonrelativistic radial wave functions $R_{nL}(r)$ which vanish as r^L at short distances. Our model may be least reliable here, and we are not very confident that either the effective cutoff momentum (~1.5 GeV) or the particular power law is correct. Nevertheless,
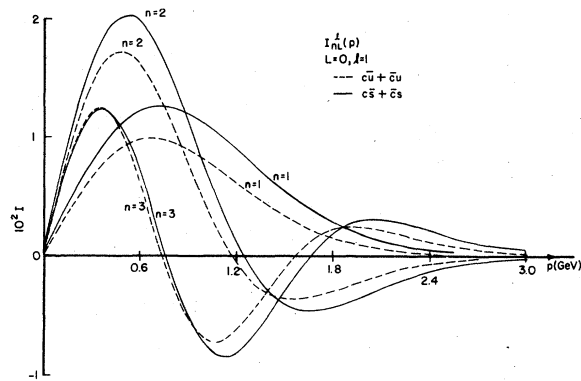
FIG. 9. P-wave decay amplitudes for $c\bar{c}$ ^3S states. The quantity plotted is $I^l_{nL}(p)$, defined in Eq. (3.37) of I where n and L are the principal quantum number and orbital angular momentum of the $c\bar{c}$ state, and l the orbital angular momentum of the decay products whose relative momentum is p. The dashed lines apply to the decays $c\bar{c} \rightarrow c\bar{u} + \bar{c}u$ (or $c\bar{d} + \bar{c}d$), the solid lines to $c\bar{c} \rightarrow c\bar{s} + \bar{c}s$; the former is therefore used for decays to nonstrange charmed mesons (e.g., $D^*\bar{D}^*$), the latter for decays involving F and/or F^*. The quark masses are $m_{u,d} = 0.335$ GeV, $m_s = 0.450$ GeV, and $m_c = 1.84$ GeV, while $a = 2.12$ GeV^{-1}. Notice that these curves differ slightly from those in Fig. 3 of I, as a result of the change in parameters described in Sec. II.

FIG. 10. P- and F-wave nonstrange decay amplitudes for $c\bar{c}$ $^3D_1$ states. Parameters are as in Fig. 9. Notice that these curves differ slightly from those in Fig. 4 of I, as a result of the change in parameters.

whatever the correct model, it will surely have decay amplitudes that fall rapidly for large momenta. Hence, any single channel can be expected to have an appreciable production cross section only within a few hundred MeV of its threshold. As W is increased, higher-mass charmed-meson states (orbital and radial excitations of D and D^*) take over from the ground states until, finally, the resonance-mediated, two-body production picture is best replaced by a continuum or parton description.

The dependence of the I^l_{nL} on the light-quark mass m_q, though complicated, is not dramatic, as we see from Figs. 9 and 10. A shift of the nodes is the most important consequence of a change in m_q.

This lengthy discussion may thus be summarized as follows: The charm production signal should be strongest at the peak of charmonium resonances. At each resonance only a few of the terms in Eq. (5.2) for the exclusive-channel ratio are important, and the relative abundances of each channel will be largely controlled by the appropriate form factor $I^l_{nL}(p_i)$.

These unprecedented features of meson production in e^+e^- annihilation will show up even more strongly in the OZI-rule-allowed decays of Υ resonances (although with a much smaller cross section). There, the first resonances above threshold will probably be 2^3D_1 (with one radial node), and 4^3S_1 (with three nodes). Furthermore, the mo-

mentum of mesons containing one heavy and one light quark increases more rapidly with W (near threshold) than it does in charm production, so there is an excellent chance of seeing rapid variations in exclusive-channel ratios. On the negative side, the splitting between hyperfine partners of the new mesons (i.e., between the 0^- and 1^- $b\bar{q}$ states) is expected to be of order 50 MeV, so that a reasonably large S-D mixing is less likely unless, by a great stroke of luck, 2^3D_1 lies in the midst of these thresholds.

B. Computed and measured cross sections

The exclusive-channel ratios R_i and their sum ΔR have been computed using parameters determined by the "renormalization" procedure[43] outlined in Sec. IV A. The omission of higher thresholds (especially those involving charmed P states) leaves the $3S$ and $4S$ resonances at too high a mass for any meaningful comparison with data. Therefore, we have artificially lowered the bare masses of these states, as well as 2^3D_1, and raised the 1^3D_1, in a crude attempt to simulate the effect of these neglected open and closed channels. The shifts we have used are

$$\Delta_{1D} = +50 \text{ MeV},$$

$$\Delta_{3S} = -80 \text{ MeV},$$

$$\Delta_{2D} = -75 \text{ MeV}, \qquad (5.7)$$

$$\Delta_{4S} = -230 \text{ MeV}.$$

The results are shown in Figs. 11–13. In Fig. 14 we also show the sum of the contributions from charm production, and from the heavy-lepton pair, $\tau\bar{\tau}$.

The published experimental data for R from the
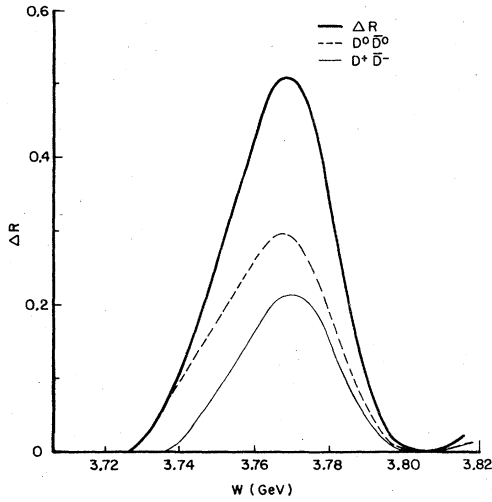
FIG. 11. The charm contribution to R in the $1\,^3D$ region (3.7 $<W<$ 3.8 GeV) as computed with the coupled-channel model. Only $D\bar{D}$ channels contribute in this energy region. Contributions from $D^0\bar{D}^0$ and D^+D^- are indicated separately.

SLAC-LBL,[44] DELCO,[45] DASP,[46] and PLUTO[47] collaborations are shown in Fig. 15. In visually comparing the various curves, one should recall that these groups make different corrections to the data, and claim somewhat different systematic errors (see Refs. 44–47). Furthermore, all data contain an uncharmed component amounting to 2–2.5 units of R, and above W= 3.564 GeV, a component from the τ lepton.[48] Given that there are differences among the various sets of data, and that our model breaks down rather badly above $W \simeq 4.3$ GeV, we shall not attempt a detailed and quantitative comparison of the model calculation with data points. Rather, we will explain the
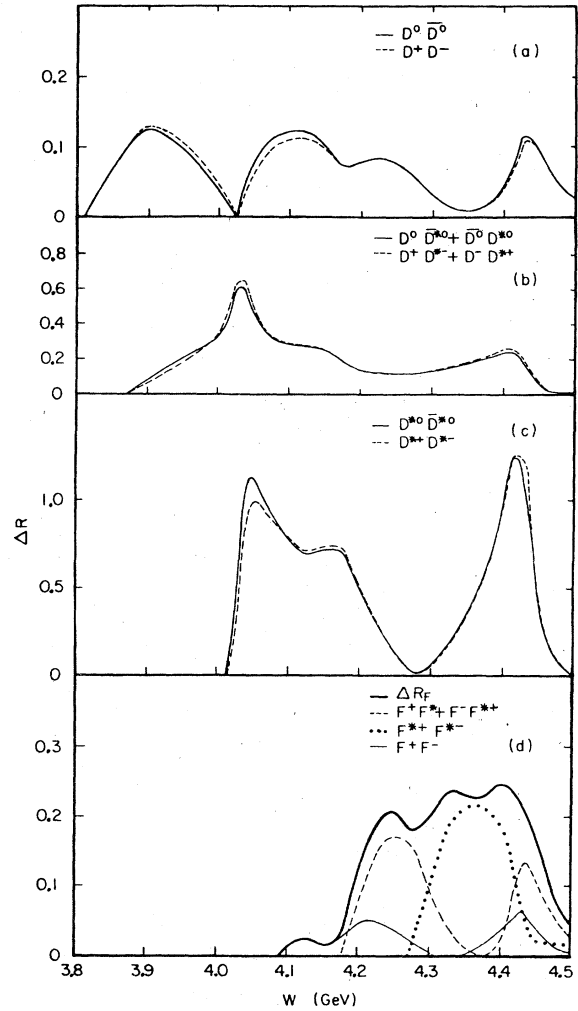
FIG. 12. The charm contribution to R from exclusive channels in the region 3.8 $<W<$ 4.5 GeV. These curves are computed from the coupled-channel model.
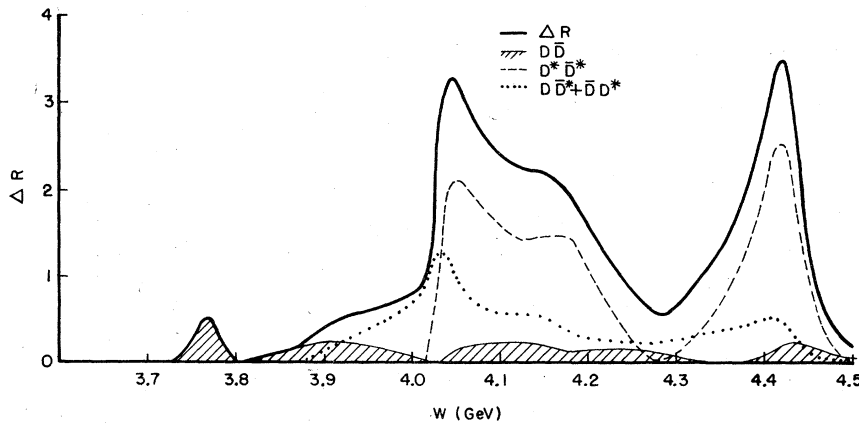
FIG. 13. The charm contribution to R in the region 3.7 $<W<$ 4.5 GeV as computed in the coupled-channel model. Contributions from F_1F_2 channels are included but not indicated separately since they are too small; they are shown in Fig. 12.
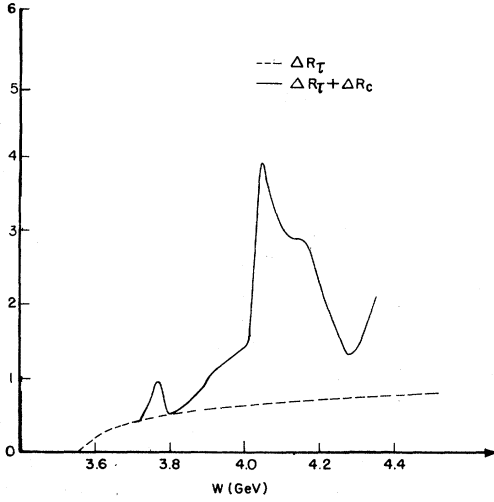
FIG. 14. Contribution to R from charm and the heavy lepton τ in the energy region $3.7 < W < 4.3$ GeV. The charm contribution is computed in the coupled-channel model, and the contribution from τ is computed assuming it is a spin-$\frac{1}{2}$ pointlike particle of unit charge and mass 1.782 GeV.

features of our curve, compare predicted widths and exclusive-channel ratios with available data, and give our interpretation of the main structures in the experimental curves.

C. $\psi(3772)$

In the region just above the charm threshold, where the only open channel is $D\bar{D}$, the charm production cross section is only significant at the resonance $\psi(3772)$. This resonance has been seen at SPEAR by both the SLAC-LBL[18] and DELCO[49] collaborations. The measured parameters from SLAC-LBL[18] are

$M = 3772 \pm 6$ MeV ,

$\Gamma = 28 \pm 5$ MeV ,

$\Gamma_{ee} = 0.37 \pm 0.09$ keV ,   (5.8)

$\Delta R(\text{peak}) = 2.18 \pm 0.34$,

while those of the DELCO group[49] are

$M = 3770 \pm 6$ MeV ,

$\Gamma = 24 \pm 5$ MeV ,   (5.9)

$\Gamma_{ee} = 0.18 \pm 0.06$ keV .

Observe that the two groups disagree on the leptonic width (or equivalently, on the height of the resonance in an R plot) by a factor of ~2.

In our model $\psi(3772)$ is the 1^3D_1 charmonium level, seen in Fig. 11 just above charm threshold. Its leptonic width stems from mixing with the 2^3S_1 $\cong \psi(3684)$, as already described in Sec. IV.
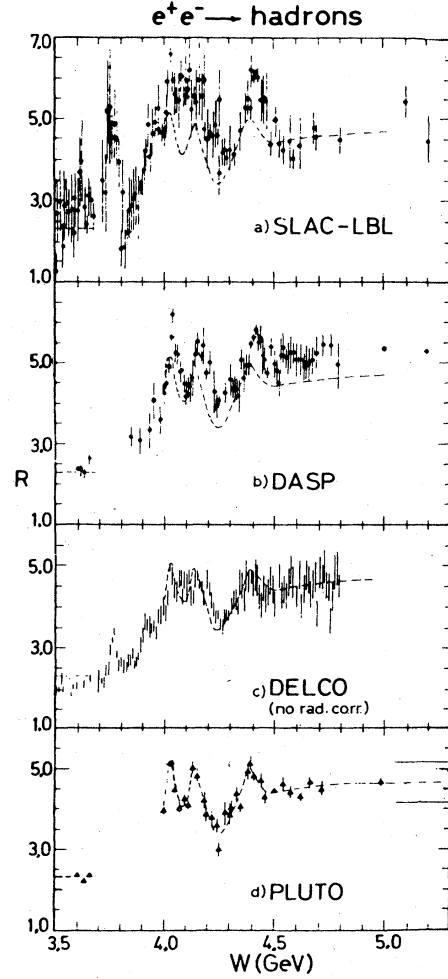
FIG. 15. Results of R (including $e^+e^- \to \tau^+\tau^-$) from four experiments: (a) SLAC-LBL (Ref. 44), (b) DASP (Ref. 46), (c) DELCO (Ref. 45), (d) PLUTO (Ref. 47). The curves represent a hand-drawn line through the PLUTO data. The band in Fig. 15(d) indicates the systematic errors of the PLUTO measurement. The plots shown were compiled by G. Feldman.

Before the discovery of the P states, or of charmed mesons, our coupled-channel calculations[50] gave a $^3D_1$ state in the vicinity of 3775 MeV, with a total width of about 30 MeV. When the D-meson masses became known, the calculations[14] were redone,[41] and gave results that correctly predicted the mass and total width of $\psi(3772)$.

The present calculation adopts a different procedure for determining the parameters in our model as described in Secs. II and III. It then turns out that 1^3D_1 lies at 3755 MeV (see Table VII)—i.e., not as close to $\psi(3772)$ as our original prediction. This illustrates a contention we have always made: The coupled-channel model cannot predict the position of resonances accurately, but

once the position is given, the other resonance parameters are predictable. In the present case this is especially obvious: We are near a threshold where very small changes in the position of a resonance lead to large variations of the predicted widths. We therefore shift the "bare" mass of the $^3D_1$ level of the potential model upward "by hand" by 50 MeV so that the pole in the coupled-channel calculation lies at 3772 MeV. The properties of $\psi(3772)$ that then emerge from this calculation are

$$\Gamma_{\text{tot}} \simeq 30 \text{ MeV},$$

$$\Gamma_{ee} \simeq 70 \text{ eV}, \qquad (5.10)$$

$$\Delta R(\text{peak}) \simeq 0.5.$$

The total width agrees very well with the data, but the leptonic width is too small [by a factor of ~2.5 or 5 depending on the experiment—cf. (5.8) and (5.9)]. Furthermore, this theoretical value of Γ_{tot} agrees with our earlier calculations[14,50] and demonstrates once again that the hadronic width is not sensitive to the details of the model if the position of the $^3D_1$ level is kept fixed at 3772 MeV. The $^3D_1$-$^3S_1$ interference, which is responsible for leptonic decay, is rather more sensitive to details, as one might expect, and the Γ_{ee} in (5.10) is a factor of 2 smaller than found in our previous calculation.

The electronic width is also sensitive to ^3S-^3D mixing due to a tensor force in the $c\bar{c}$ potential itself, even though this mixing is much smaller than that due to virtual and real decay. To see this, we briefly consider this effect under the assumption that our confining potential (2.1) arises from the exchange of a Lorentz vector. It then leads to a tensor force in the Breit Hamiltonian having the matrix elements[51]:

$$\langle 2^3S | V_T^{\text{Coul}} | 1^3D \rangle = 1.9 \text{ MeV},$$
$$\langle 2^3S | V_T^{\text{lin}} | 1^3D \rangle = -4.9 \text{ MeV}. \qquad (5.11)$$

Equation (5.11) predicts the following mixing angles and electronic widths:

Coulomb: $\theta = 1.2°$, $\Gamma_{ee} = 1.0$ eV,
linear: $\theta = -3.2°$, $\Gamma_{ee} = 6.5$ eV. $\qquad (5.12a)$

These should be compared with the coupled-channel results:

coupled channel: $\theta = -10°$, $\Gamma_{ee} = 70$ eV. $\qquad (5.12b)$

The relative signs of the mixing angles are determined from the behavior of R when a tensor force in the potential is incorportated into the coupled-channel calculations.

The leptonic width of $\psi(3772)$ is also sensitive

to relativistic corrections to the ^3D wave function.[4] If Γ_{ee}^0 is the leptonic width due to S-D mixing alone, this relativistic correction has the form

$$\Gamma_{ee} = \Gamma_{ee}^0 \left[1 - \cot\theta \frac{5}{6\sqrt{2}} (m_c a)^{-4/3} \left(\frac{u_D'''(\rho)}{u_s'(\rho)} \right)_{\rho=0} \right]^2,$$
$$(5.13)$$

where $u(\rho)$ is the radial wave function defined in I. For our parameters this more than doubles the theoretical rate to ~160 eV, which is then in better agreement with the data than the values quoted above. What is not really clear is whether other relativistic corrections are of comparable importance.

The tensor force due to a Coulomb potential decreases the S-D mixing of the coupled-channel calculation by a very small amount; that due to a linear potential increases the S-D mixing substantially. According to (5.13) the electronic width Γ_{ee} in the latter case would be 0.23 keV, which is only 1.5 standard deviations below the SLAC-LBL result. It is therefore conceivable that the discrepancy between our calculation of Γ_{ee} and the data may be removed by a tensor force in the $c\bar{c}$ potential. On the other hand, our results for the hadronic width are far less sensitive to such a tensor force.

Although it is now well known, we repeat[14] that the ψ'' peak is by far the best place to study properties of D^0 and D^+ because there is no clutter from extra pions and photons from D^* and higher charmed-meson decays. In studying F's and the new mesons associated with Υ, a similar resonance—decaying exclusively to the ground-state pseudoscalars—should be sought out. In the case of F^+, the only hope is at the peak of the apparent resonance at 4.16 GeV (see below).

If the D^0 and D^+ cross sections at ψ'' can be measured with sufficient precision, it may be possible to observe the effects of the $^3D_1$ form factor $I_{12}^1(p_D)$. On the basis of isospin conservation and phase space alone, one expects

$$\frac{\sigma(e^+e^- \to D^0\bar{D}^0)}{\sigma(e^+e^- \to D^+D^-)} = \left(\frac{p_{D^0}}{p_{D^+}} \right)^3 = 1.45. \qquad (5.14)$$

However, our model predicts (see Fig. 11) that at the resonance peak

$$\frac{\sigma(e^+e^- \to D^0\bar{D}^0)}{\sigma(e^+e^- \to D^+D^-)} = 1.36, \qquad (5.15)$$

a small, but hopefully measurable effect.

ΔR dips to zero near 3.8 GeV in Fig. 11 because charm production in our model is vector-meson dominated and there is no resonance here. This, too, agrees well with the SPEAR results, especially when one allows for a small amount of τ production in the data ($\Delta R_\tau \simeq 0.5$).

D. Exclusive-channel ratios above $W = 3.8$ GeV

In our calculation there is some weak structure in the 3.9–4.0 GeV region. It does not arise from a $c\bar{c}$ resonance, but from the opening of the $D\bar{D}^* + D^*\bar{D}$ channel and a decrease in the $D\bar{D}$ channel due to a nearby zero in the $3S$ decay amplitude. This can be tested by measuring the ratios of $D\bar{D}$ to $D\bar{D}^*$ exclusive channels in the 3.9–4.1 GeV region, where a dip approaching zero should occur.

The measurements of R show quite pronounced structures in the 3.9–4.0 GeV region (see Fig. 15), but there are obvious disagreements between experiments. Consequently we cannot say whether our model agrees with these data or not. As there is a very important point at stake here, we shall return to this energy region in Sec. V E below.

Another manifestation of vector-meson dominance is seen by comparing $D^*\bar{D}$ and $D^*\bar{D}^*$ production near $W = 4$ GeV. In our model, most charm production from about 3.9 to 4.15 GeV proceeds through the 3^3S_1 level, seen in Figs. 12 and 13 as the prominent peak at 4.05 GeV. With a threshold fairly far from the $3S$ pole, the $D^*\bar{D}$ channel turns on with a very gradual p^3 rise, and does not become appreciable until the pole is reached. The $D^*\bar{D}^*$ channel starts just below the $3S$ pole, and the limited phase space for decay into this channel makes the $3S$ fairly narrow. Thus, ΔR increases rapidly as the pole is approached, as does $D^*\bar{D}^*$ production. Finally, $D\bar{D}$ production nearly vanishes at 4.025 GeV (in this calculation) because $I^1_{30}(p)$ has a zero at $p_D = 750$ MeV.

These peculiarities of charm production are consistent with the data of the SLAC-LBL group taken at the peak of the resonance at 4.028 GeV, which we interpret as the (mostly) 3^3S_1 charmonium state. In particular, they find[34]

$$R_{D^*0\bar{D}^*0} : R_{D^*0\bar{D}^0 + D^0\bar{D}^*0} : R_{D^0\bar{D}^0}$$

$$= 1.00 \pm 0.10 : 0.85 \pm 0.09 : 0.10 \pm 0.06. \quad (5.16)$$

The corresponding ratios for charged-D produc-

tion are not known yet. On the basis of the naive 7:4:1 rule, one would estimate the ratios in Eq. (5.16) to be

$$7p_{D^*0\bar{D}^*0}^3 : 4p_{D^*0\bar{D}^0}^3 : 1p_{D^0\bar{D}^0}^3 = 1.0 : 17.4 : 11.1.$$

$$(5.17)$$

Even allowing for a naive monotonic momentum cutoff, say $\exp[-(p/500 \text{ MeV})^2]$, the relative ratios are $1.0 : 5.6 : 1.2$, still in gross disagreement with experiment. This fact has led several authors[36] to interpret $\psi(4028)$ as a "$D^*\bar{D}^*$ molecule," an almost bound state of these two charmed mesons. There is no need for this *ad hoc* hypothesis; these unexpected ratios can be accounted for by the zero in $I^1_{30}(p_{D^0}\bar{D}^0)$. At the peak of the 3^3S_1 resonance in Fig. 13, we find from Fig. 12

$$R_{D^*0\bar{D}^*0} : R_{D^*0\bar{D}^0 + D^0\bar{D}^*0} : R_{D^0\bar{D}^0} = 1.0 : 1.35 : 0.005$$

$$(5.18)$$

and

$$R_{D^{*+}D^{*-}} : R_{D^{*+}D^- + D^+D^{*-}} : R_{D^+D^-} = 1.0 : 2.69 : 0.004.$$

$$(5.19)$$

The last numbers in (5.18) and (5.19) are not to be taken too seriously because $R_{D\bar{D}}$ varies rapidly when p_D is close to zero of I^1_{nL}. What is certain is that $R_{D\bar{D}}$ is small here. The node has resulted in an enormous suppression of $D\bar{D}$ compared to $D^*\bar{D}^*$ even though the latter is just 14 MeV above its threshold. Thus the oscillatory form factor gives at least a qualitative explanation[41,42,50] of the ratios (5.16). These oscillations are a direct consequence of the radial nodes in the $3S$ $c\bar{c}$ wave function. The existence of the node in the decay amplitude is therefore an issue of rather fundamental importance, and should be settled as unambiguously as possible by further measurements.

From the D^* branching ratios calculated in the Appendix, and defining $B^+_{r+} = B(D^{*+} \to D^0\pi^+)$, etc., we predict[52]

$$\sigma(e^+e^- \to D^0 + \text{any})/\sigma(e^+e^- \to D^+ + \text{any}) = [R_{D^0\bar{D}^0} + (1 + B^0_{r0} + B^0_\gamma)R_{D^*0\bar{D}^0} + (B^0_{r0} + B^0_\gamma)R_{D^0\bar{D}^*0}$$

$$+ B^+_{r+}(R_{D^{*+}D^-} + R_{D^{*+}D^{*-}})]$$

$$\times [R_{D^+D^-} + (1 + B^+_{r0} + B^+_\gamma)R_{D^{*+}D^-} + (B^+_{r0} + B^+_\gamma)R_{D^{*+}D^{*-}}]^{-1}$$

$$= 2.84 \quad\quad\quad\quad (5.20)$$

at $W = 4.028$ GeV. [In Eq. (5.20), $R_{D^*\bar{D}}$ $= \frac{1}{2}(R_{D^*\bar{D}+D\bar{D}^*})$.]

Our assignment of $\psi(4028)$ to the $3S$ state can be tested experimentally. The decay amplitudes depend on the orbital angular momentum L of the initial state and thus distinguish an S state from a D state. In particular, at the same momentum

the ratio of decay rates for $D\bar{D}$ to $D\bar{D}^* + D^*\bar{D}$ is given by

$$B_D \equiv \frac{\text{rate for } D\bar{D}}{\text{rate for } D\bar{D}^* + \bar{D}D^*} = \begin{cases} \frac{1}{4} & \text{for } L = 0 \ (S \text{ state}), \\ 1 & \text{for } L = 2 \ (D \text{ state}). \end{cases}$$

$$(5.21)$$

TABLE XII. Methods of distinguishing different interpretations of 4.16-GeV structure. The definition of B_D is given by Eq. (5.21) in the text.

| Observables | Possible interpretation of 4.16-GeV structure | | |
	2D state	4S state	Threshold structure
Behavior of B_D in the 4.1 to 4.2 GeV region	Increases sharply by factor ~3–4	Slowly varying	Slowly varying
Minimum in R between 4.03 and 4.16 GeV	Cannot vanish	May vanish	May vanish
Opening of a new threshold	Not necessary	Not necessary	Must be a major fraction of charmed states at 4.16 GeV

This test is complicated by the difference in D and D^* masses which leads to different momenta for the two decays at the same total energy. The 4.028 state however fits well as the 3S state when the momentum difference is taken into account. Then the expected value is $B_D \lesssim \frac{1}{10}$ for an S state and $B_D \sim \frac{1}{3}$ for a D state, while the measured ratio[34,45] at 4.028 GeV is $B_D \leq \frac{1}{10}$.

As explained previously, beyond ~4.3 GeV our model calculation breaks down. The small structure in our computed R at 4.16 GeV is due to the 2^3D_1 charmonium level, mixed with 3^3S_1. The potential model discussed in Sec. II also places the 2D at 4.19 GeV. Therefore, we interpret the apparent resonance seen in Fig. 15 near 4.16 GeV as the 2D state. In the coupled-channel calculation, we find very little mixing with the 3S state because there are no important nearby thresholds; in particular, F production is only about 1% of D production in this region.

There are two other possible interpretations of the 4.16-GeV structure: (i) as the 4S state favored by the logarithmic-potential model; (ii) as a threshold structure similar to that at 3.95 GeV. When better data become available, these can be distinguished by the considerations given in Table XII.

Finally, we briefly consider the structure observed in the 4.4-GeV region. The dip at 4.28 GeV seen in Fig. 15 suggests that the 4.4-GeV object is a new S-state resonance that is not strongly coupled to the resonances in the 3.9–4.2 GeV region. We also emphasize that many new thresholds open in this region, in particular those for p-wave charmed mesons. For the latter we use the notation $D(P_{j,J})$, where j is the total angular momentum of the light quark. Thus $D^*\bar{D}(P)$ + $\bar{D}^*D(P)$ and $D(P)\bar{D} + \bar{D}(P)D$ are expected to be important. Of these $D(P_{1/2,1})\bar{D} + \bar{D}(P_{1/2,1})D$ might

be especially prominent because of its large statistical weight and available phase space. $D(P_{1/2,1})$ decays strongly into $D^*\pi$, and is therefore expected to have a normal hadronic width. At $W=4.415$ GeV there is such an enhancement observed[34] in the recoil spectrum of D^0 at a mass of 2.45 GeV [roughly the expected mass of the $D(P_{1/2,1})$ state shown in Fig. 18].

In the Appendix we have estimated the masses of the excited charmed mesons. The results are shown in Figs. 17 and 18. We find that the first charmed P states are approximately 250 MeV below the first radial excitations of the S-wave charmed mesons. Thus, $D\bar{D}(P)$ and $D^*\bar{D}(P)$ are the new low-lying thresholds that occur in the 4.2–4.5 GeV region. Properties of these new channels are listed in Table XIII.

TABLE XIII. New open channels in e^+e^- annihilation in the 4.2 to 4.5 GeV region. The notation $D(P_{j,J})$ denotes a P-state charmed meson of spin J, and j is the total angular momentum of the light quark. These masses are for the neutral mesons.

Channel	Mass (GeV)	Threshold behavior	Statistical factor
$D\bar{D}(P_{1/2,0})$	4.22	Forbidden	
$D\bar{D}(P_{1/2,1})$	4.23	S wave	$\frac{2}{3}$
$D^*\bar{D}(P_{1/2,0})$	4.36	S wave	$\frac{2}{3}$
$D^*\bar{D}(P_{1/2,1})$	4.37	S wave	$\frac{4}{3}$
$D\bar{D}(P_{3/2,2})$	4.37	D wave	$\frac{2}{3}$
$D\bar{D}(P_{3/2,1})$	4.36	D wave	$\frac{2}{3}$
$D^*\bar{D}(P_{3/2,1})$	4.51	D wave	$\frac{4}{3}$
$D^*\bar{D}(P_{3/2,2})$	4.52	D wave	$\frac{8}{3}$

E. Is there an unaccounted-for resonance between $\psi(3772)$ and $\psi(4030)$?

As already remarked in Sec. VD, all measurements in the 3.9–4.0 GeV region indicate the existence of an enhancement in R. Unfortunately the experiments do not agree on the location of this structure, nor on its shape. Our model gives considerable variations of R in this region for reasons explained in Sec. VD. Should this not suffice, small *ad hoc* modifications in the decay amplitudes can be shown to give quite pronounced structures in R in this region (see Fig. 12 of Ref. 2). But, if there is really a well-defined resonance between 1^3D_1 and 3^3S_1 [i.e., between $\psi(3772)$ and $\psi(4030)$], our model simply cannot account for it. On the other hand, there is a plausible candidate for a narrow state in this region: the lowest-lying vibration of the gauge field binding the $c\bar{c}$ pair.[53]

A careful measurement of R in the interval 3.9–4.0 GeV is therefore of great importance. It is probably the most favorable place to find clearcut evidence for gluon excitations, because the next excited states, which are expected to lie near 4.4 GeV in the model of Giles and Tye,[53] fall in a region where our understanding of the $c\bar{c}$ states, and of their decay, is already quite poor, and an unambiguous interpretation of the data may be very difficult to achieve.

If the sectors discussed in this paper and those where gluons are excited are not strongly coupled, our predictions for the exclusive branching ratios should be valid except, of course, in the immediate vicinity of resonances associated with excitations of the gauge field.

VI. SUMMARY AND CONCLUSIONS

In this paper we have presented a detailed comparison of the naive and coupled-channel models formulated in I with the available data, and made a number of predictions. These may be summarized as follows.

A. Naive $Q\bar{Q}$ model

(1) The linear plus Coulomb potential model gives a good account of the observed spectrum in both the ψ and Υ families. To achieve this one must use the observed ^3P $c\bar{c}$ levels as an input, instead of the leptonic width Γ_e of ψ and/or ψ'.

(2) This suggests that the van Royen-Weisskopf formula for Γ_e is unreliable, as indicated independently by a simple transcription to QCD of radiative corrections in QED. These corrections are approximately state independent, and one therefore expects the model to account for *ratios* of leptonic

widths. We indeed find that Γ_e for ψ', Υ, and Υ' are all given correctly by the model in terms of $\Gamma(\psi \to e^+e^-)$.

(3) $E1$ rates predicted by the $c\bar{c}$ model for $\psi' \to {}^3P$ are systematically too large by a factor of 2. We do not consider this a serious discrepancy as $E1$ rates are very sensitive to wave-function details. Predictions for a large number of $E1$ transitions in the Υ spectrum are given; presumably they too are only reliable to within a factor of 2.

(4) Now that $X(2820)$ seems to have disappeared from the scene, and there are indications that $\chi(3450)$ will follow suit, the only serious blemishes on the face of the charmonium model appear to have been removed. Naturally it is still very important to find the hyperfine partners of ψ and ψ'. But we must now presume that the hyperfine splittings are as small as theory has always indicated, and this makes the observation of the $M1$ transitions that will disclose the ^1S states difficult.[21a]

(5) The naive model is also remarkably successful when applied to $Q\bar{q}$ mesons, where Q is a quark much heavier than q. As shown in the Appendix, the low-lying states of these "heavy-light" systems are well described by a semiempirical mass formula with relatively few parameters.

B. Coupled-channel model

Incorporation of coupling to charmed-meson decay channels by a very simple extension of the naive $c\bar{c}$ model leads to a qualitative understanding of many of the phenomena observed above the charm threshold, and confirms that the naive model provides an adequate description of below-threshold phenomena.

(1) Below charm threshold, mixing between $c\bar{c}$ states and the charmed-meson sector is rather small, and leads to modest (~20%) reductions in the $E1$ rates predicted by the naive model. The leptonic width of ψ' that emerges from the coupled-channel calculation is in complete agreement with experiment.

(2) The model gives a quite complete understanding of $\psi(3772)$ as the $^3D_1$ $c\bar{c}$ state mixed with 2^3S by both open and closed decay channels.

(3) The decay amplitudes for $c\bar{c} \to \bar{c}q + q\bar{c}$ are oscillatory functions of momentum, with a node structure that is determined by the radial nodes in the $c\bar{c}$ wave function. This provides a qualitative understanding of the peculiar branching ratios into various charmed-meson channels observed at 4.03 GeV. The prediction of a zero in $\sigma(e^+e^- \to D\bar{D})$ near 4.0 GeV should be tested experimentally because it would, for the first time, confirm in detail the structure of a quark-antiquark radial wave function.

(4) More reliable measurements of R between

$\psi(3772)$ and $\psi(4030)$ are needed. Our model predicts modest variations of R in this region because of a variety of threshold and decay effects, but the present data hint at the existence of a much more marked structure. The discovery of a sharp resonance in this region would have considerable significance, for it would reveal degrees of freedom that cannot be described by the charmonium model as it stands. The latter has no room for a level between 1^3D_1 and 3^3S, i.e., between $\psi(3772)$ and $\psi(4030)$.

The spectroscopy of the Υ family will afford new and more stringent tests of the model presented here. We hope that this new spectroscopy will provide better clues concerning the relationship of the phenomenological model to QCD itself.

Note added in proof.

(1) The charmonium ground state η_c appears finally to have been found by the Crystal Ball Collaboration at SPEAR (C. Peck, invited paper, Montreal Meeting of the APS Division of Particles and Fields, 1979 (unpublished). Its essential properties are $m(\eta_c) = 2.977 \pm 0.003$ GeV and $\Gamma(\psi \to \gamma\eta_c) \simeq \Gamma(\psi' - \gamma\eta_c) \simeq 0.7$ keV; as yet there is no quoted error for these rates. According to our Eq. (2.8), $\Gamma(\psi \to \gamma\eta_c) = 2.0$ keV. For hindered $M1$ transitions, Γ_{M1} varies approximately like k^7; from Table II we then find that $\Gamma(\psi' \to \gamma\eta_c) = 1.0$ keV. It is puzzling that the theory agrees so well with the preliminary data for the hindered transition, which is very sensitive to wave-function details, whereas it disagrees significantly with the model-insensitive allowed transition. Since the experimental rates quoted above assume the total widths of the η_c to be smaller than the photon-energy resolution, one possible solution to this disagreement is that the widths of the η_c are considerably larger than anticipated. For example, if the total widths of the η_c are found to be 15–20 MeV, the resulting experimental rate $\Gamma(\psi \to \gamma\eta_c)$ is roughly tripled while the rate $\Gamma(\psi \to \gamma'\eta_c)$ remains essentially unchanged.

(2) A third narrow Υ resonance has been discovered at the Cornell storage ring CESR by the CLEO and Columbia–Stony Brook collaborations (B. D. McDaniel, private communication). Called Υ'', it is presumably $3^3S(b\bar{b})$. Its observed excitation energy is $m(\Upsilon'') - m(\Upsilon) = 891$ MeV. As we saw in Sec. IID, when the *same* potential is used for the $b\bar{b}$ and $c\bar{c}$ systems, the $2S$-$1S$ $b\bar{b}$ separation of 591 MeV is some 5% larger than the observed value of $m(\Upsilon') - m(\Upsilon)$. One can "fine tune" our model to give the observed $2S$-$1S$ spacing by introducing a small flavor dependence into the Coulombic term of the potential. This is achieved by reducing κ to 0.48 from 0.52, while keeping m_b and a at their previous values of 5.17 GeV and 2.34 GeV^{-1}, respectively. [Note that a reduction of κ is what one

would expect from asymptotic freedom, though as we saw in Eq. (2.27), a naive estimate leads to a much larger reduction.] With this slightly modified model, one finds that $m(\Upsilon') - m(\Upsilon) = 898$ MeV, in excellent agreement with the CESR observation; the $4S$ level, at 10.63 GeV, is expected to be above the OZI threshold. In view of the forthcoming measurements at CESR, we list below the modified excitation energies and leptonic widths of the Υ family; these replace Table IV in the text. (Quantities bearing an asterisk are inputs.)

State	Δ_m (MeV)	Γ_{ee} (keV)
$1S$	0*	1.24*
$1P$	463	
$2S$	560*	0.48
$1D$	705	
$2P$	811	
$3S$	898	0.34
$2D$	995	
$4S$	1170	0.28
$3D$	1245	
$5S$	1410	

After fine tuning, many other models[9-11] give very similar predictions for the $3S$ and $4S$ positions. For a new and successful model that uses a Coulombic term incorporating the running coupling constant, see J. L. Richardson, Phys. Lett. 82B, 272 (1979).

APPENDIX: PROPERTIES OF CHARMED MESONS

The nonrelativistic treatment developed for the $c\bar{c}$ bound states in Paper I, and in Sec. II of this paper, cannot be expected to work well for mesons $c\bar{q}$ whose lighter constituent q should be treated relativistically. To develop an adequate dynamical theory of charmed mesons, on the other hand, is certainly beyond the scope of this article. Instead, the intent of this Appendix is to obtain rough esti-

mates of the mass spectrum and decay properties of the charmed-meson system needed in the text. The experimental data on charmed mesons are employed wherever possible; those properties which are not available experimentally at present are estimated by relying heavily on the analogy with the K-meson family.

1. Mass spectrum

The following charmed-meson masses are presently known experimentally[16]:

$$m(D^0) = 1.8633 \pm 0.0003 \text{ GeV},$$
$$m(D^+) = 1.8684 \pm 0.0004 \text{ GeV},$$
$$m(D^{*0}) = 2.0062 \pm 0.0025 \text{ GeV}, \qquad \text{(A1)}$$
$$m(D^{*+}) = 2.0086 \pm 0.0005 \text{ GeV}$$
$$= m(D^0) + 0.1453 \pm 0.0005 \text{ GeV}.$$

If one is to apply the coupled-channel model to the ψ system, one must know the quasi-two-body charmed-meson thresholds, and thus the masses of the excited states of the $c\bar{q}$ system.

The reduced mass of the $c\bar{q}$ system is only ~0.3 GeV which points to the danger of applying the nonrelativistic potential model of Sec. II. Furthermore, the experimental hyperfine splitting of the D and D^* evident in (A1) demonstrates that spin-dependent corrections to the nonrelativistic spectrum may be substantial. As we have seen in

Sec. II, however, the description of fine and hyperfine structure is not very satisfactory even for the much more nonrelativistic $c\bar{c}$ system. For these reasons it is difficult to obtain the excitation spectrum of $c\bar{q}$ systems by dynamical calculations. Instead, we shall make a crude estimate by exploiting the similarity between $c\bar{u}$ and $s\bar{u}$ as heavy-quark–light-quark systems.

According to nonrelativistic quantum mechanics, the energy of a two-body system depends on the particle mass only through the reduced mass combination $\mu = m_Q m_q/(m_Q + m_q) = m_q - (m_q^2/m_Q) + O(m_q^3/m_Q^2)$, where m_Q, m_q are the masses of the heavy (Q) and light quarks (q), respectively. Since μ becomes independent of m_Q as $m_Q \rightarrow \infty$, the dynamics of a $Q\bar{q}$ system is completely determined in this limit by the light constituent. The corrections due to finite m_Q are partly given by the second term of μ, which represents the recoil correction of the heavy quark. Hyperfine interactions (spin-spin) and tensor forces also vary with m_Q as $1/m_Q$. The spin-orbit interaction has a piece independent of m_Q which survives in the limit $m_Q \rightarrow \infty$.

Taking these interactions into account, and assuming quark mass independence of the effective potential (see Sec. II), one may write down a general form for the mass spectrum of $Q\bar{q}$ systems[54]:

$$m(n; l; J^{PC}; m_Q^{-1}) = m_0 + [\epsilon_0(n,l) + \vec{L} \cdot \vec{S}_q \epsilon_{LS}^0(n,l)]$$

$$+ \frac{m_q^2}{m_Q}[\vec{S}_Q \cdot \vec{S}_q \epsilon_{SS}^0(n,l) + T_{12}\epsilon_T^0(n,l) + \vec{L} \cdot (\vec{S}_q + \vec{S}_Q)\epsilon_{LS}^1(n,l) + \epsilon_1(n,l)] + O(m_q^3/m_Q^2), \qquad \text{(A2)}$$

where

$$T_{12} = \langle nJlj|[(\vec{S}_Q \cdot \hat{r})(\vec{S}_q \cdot \hat{r}) - \tfrac{1}{3}\vec{S}_Q \cdot \vec{S}_q]|nJlj\rangle. \qquad \text{(A3)}$$

Equation (A2) is simply an expansion of the meson mass in powers of $1/m_Q$ with the following definition of the terms involved: m_0 is the mass of the lowest state in the spectrum when $1/m_Q$ corrections are ignored; ϵ_0 is the basic excitation energy in the limit $1/m_Q \rightarrow 0$ and ϵ_{LS}^0 gives the spin-orbit splitting of multiplets in the same limit; the terms ϵ_{SS}^0 and ϵ_T^0 represent the leading spin-spin and tensor force corrections; finally, ϵ_1 and ϵ_{LS}^1 denote the $1/m_Q$ corrections to the order zero terms; i.e., the recoil correction and the $1/m_Q$ part of the spin-orbit force.

In Eq. (A2) it is explicit that the multiplet splitting in the limit $m_Q \rightarrow \infty$ depends only on $\vec{j} = \vec{L} + \vec{S}_q$, the total angular momentum of the light quark. The proper classification of $Q\bar{q}$ multiplet splittings is in terms of j, rather than $S(\vec{S} = \vec{S}_Q + \vec{S}_q)$, as in the case of $Q\bar{Q}$ systems. Thus, the two $J=1$ P states of the $c\bar{q}$ system should be specified by $j = \frac{1}{2}, \frac{3}{2}$ and not by $S = 0, 1$. We therefore use the notation

$nL_{j,J}$ for $Q\bar{q}$ states.

There have been numerous discussions of the terms of (A2) in the context of specific models.[55] However, for our applications only the general form of these terms will be needed.

In order to estimate the $c\bar{q}$ excitation spectrum by (A2), we will assume that the $s\bar{u}$ (K-meson) system can also be treated as a $Q\bar{q}$ system. This is difficult to justify since m_s is only ~0.5 GeV; nevertheless there is some indication that this is not such a bad approximation. In particular, the relation

$$[m(D^*) - m(D)] \simeq (m_s/m_c)[m(K^*) - m(K)], \qquad \text{(A4)}$$

which follows from (A2), is reasonably well satisfied by the observed "hyperfine" splittings between K, K^* and D, D^*.

Presumably, formula (A2) applies reasonably well to the $c\bar{q}$ system itself. Once the $c\bar{q}$ spectrum is known experimentally, Eq. (A2) should provide a reliable guide to the spectroscopy of mesons containing a b quark, or still heavier quarks.

We now turn to the actual estimation of the mass spectrum of $c\bar{q}$ systems. Figure 16 shows the observed mass spectrum of the $s\bar{u}$ (or $s\bar{d}$) system. There is a substantial experimental uncertainty in the identification of the P-state levels.[56] But let us accept the level assignments of Fig. 16, and estimate the various terms in (A2). Then the center of gravity (c.o.g.) of the $1S$ and $1P$ states are 0.79 GeV and ~1.35 GeV, respectively. This observed $1P$-$1S$ difference of 0.56 GeV is in remarkably good agreement with the nonrelativistic model of Sec. II, which yields 0.53 GeV. There is equally good agreement between the observed (1.0 GeV) and model (0.95 GeV) values of the $1D$-$1S$ separation. [In this case we use the reduced mass $\mu = 0.19$ GeV, and the parameter set A of Eq. (2.4).] We shall therefore use the potential model values of $\epsilon_0(n, l)$ of the $c\bar{q}$ system (in particular, to give the c.o.g. of the radial excitation). The resulting spectrum is shown in Fig. 17.

Next we estimate the splitting of levels due to spin-dependent forces. The distance between the c.o.g. of $P_{3/2}$ and $P_{1/2}$ states in the K-meson

spectrum of Fig. 16 leads to

$$\epsilon^0_{LS}(1, 1) = 0.10 \text{ GeV} . \tag{A5}$$

Since we have not enough information to evaluate ϵ^0_{SS}, ϵ^0_T, etc., separately, we shall simply assume that the splitting of $K^*(1420)$ and Q_2, and that of κ and Q_1, are due to forces proportional to m_q/m_Q. Then the $P_{3/2,2}$-$P_{1/2,1}$ and $P_{1/2,1}$-$P_{1/2,0}$ splitting of the $c\bar{u}$ system are obtained by reducing the K-meson splittings by $m_s/m_c \sim \frac{1}{4}$.

Finally we determine m_0. For the lowest states D^0 and D^{*0} in the $c\bar{u}$ spectrum, Eq. (A2) gives

$$m(D^0) = m_0 - \tfrac{1}{4}(m_u/m_c)\Delta E ,$$

$$m(D^{*0}) = m_0 + \tfrac{3}{4}(m_u/m_c)\Delta E ,$$

where ΔE is positive. Thus

$$m_0 = [3m(D^{*0}) + m(D^0)]/4 = 1.970 \text{ GeV} . \tag{A6}$$

The mass spectrum of the $c\bar{q}$ system calculated from (A2), (A5), and (A6) is shown in Fig. 18. In particular, our estimate of the lightest charmed P-state masses are
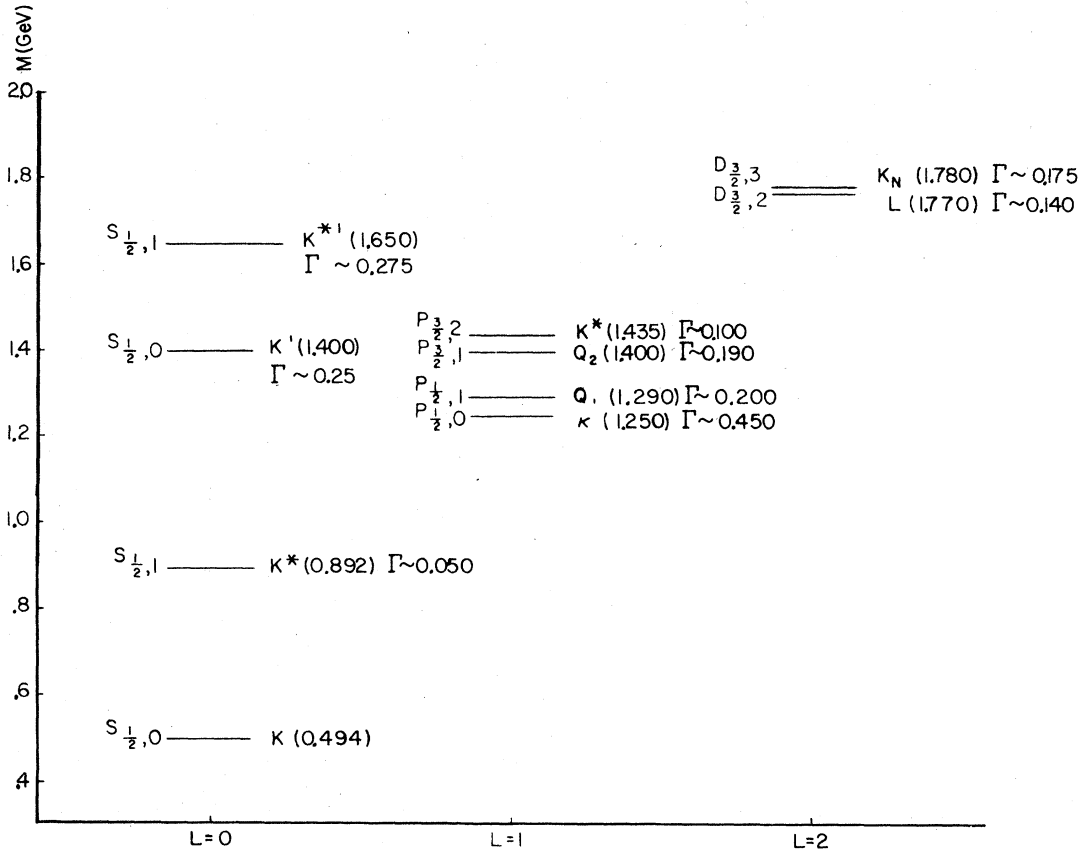
FIG. 16. Experimental strange-meson spectrum. Masses are given by the numbers in GeV in the brackets. Γ is the width in GeV. The spectroscopic notation is $nL_{j,J}$ where j is the total angular momentum of the light quark: $\vec{j} = \vec{S}_q + \vec{L}$.
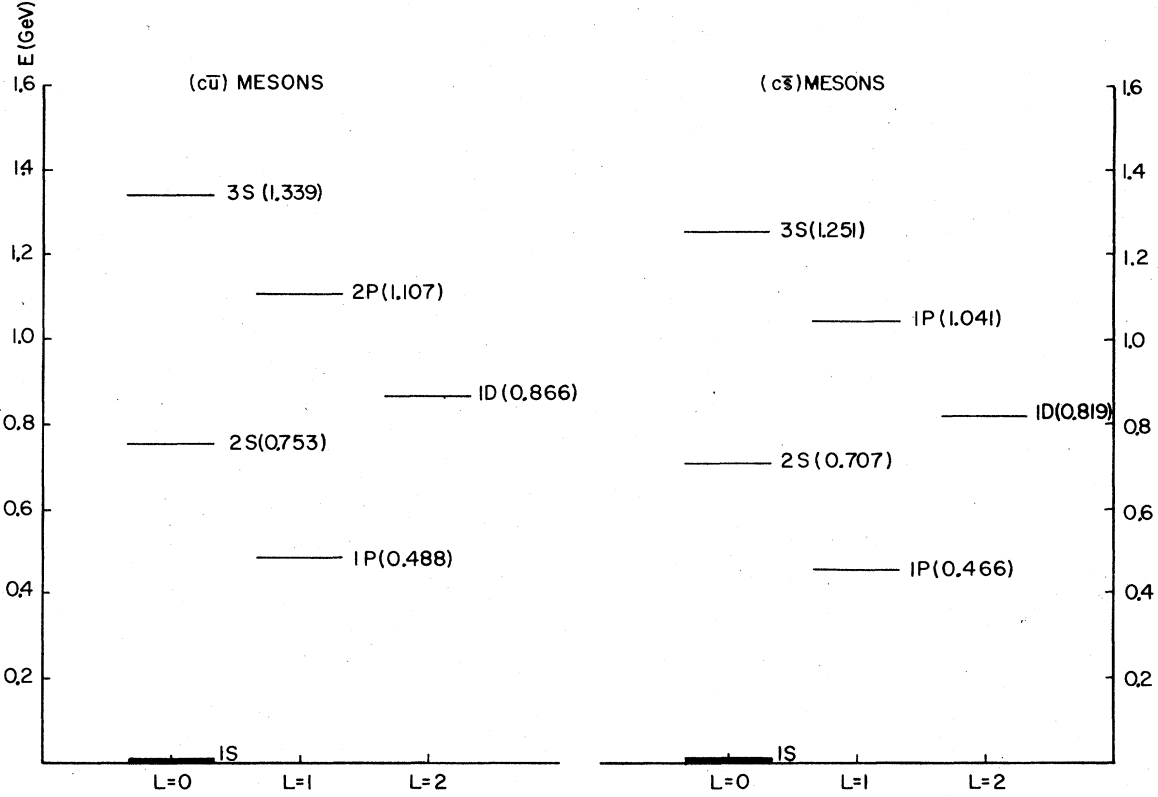
FIG. 17. Theoretical radial and orbital excitation spectrum of charmed mesons. Notation is the same as in Fig. 16.

$M(1P_{1/2,0}) = 2.354$ GeV,

$M(1P_{1/2,1}) = 2.364$ GeV,

$M(1P_{3/2,1}) = 2.503$ GeV,   (A7)

$M(1P_{3/2,2}) = 2.511$ GeV.

The lowest masses of F mesons can be estimated using the naive quark model:

$m(F^*) = m(D^*) + m(\phi) - m(K^*) = 2.135$ GeV,

$m(F) = m(F^*) - [m(D^*) - m(D)] = 1.994$ GeV.

(A8)

They agree with the observed[20] values 2.14 ± 0.06 GeV and 2.03 ± 0.06 GeV.

2. Radiative and hadronic transitions among charmed mesons

For the discussion of inclusive production of D^0 and D^+ in Sec. V we need the branching ratios of $D^{*0} \to D^0 + (\pi^0, \gamma)$, $D^{*0} \to D^+ + \pi^-$, $D^{*+} \to D^+ + (\pi^0, \gamma)$, and $D^{*+} \to D^0 + \pi^+$. Here we estimate the radiative and hadronic transitions of low-lying charmed mesons.

The extremely small Q values for the decays $D^* \to D\pi$ make these rates very sensitive to the

precise values of D and D^* masses. Using just isospin, phase space, and the observed charmed-meson masses given in (A1), we find

$$\frac{\Gamma(D^{*+} \to D^+ + \pi^0)}{\Gamma(D^{*+} \to D^0 + \pi^+)} = 0.42 \pm 0.12 \qquad (A9a)$$

and

$$\frac{\Gamma(D^{*+} \to D^0 + \pi^+)}{\Gamma(D^{*0} \to D^0 + \pi^0)} = 1.27^{+0.98}_{-0.50}. \qquad (A9b)$$

These errors reflect the sensitivity to Q values.

The decay $D^{*0} \to D^+\pi^-$ is forbidden or very nearly forbidden kinematically; with the errors quoted in (A1)

$$\frac{\Gamma(D^{*0} \to D^+ + \pi^-)}{\Gamma(D^{*0} \to D^0 + \pi^0)} \lesssim 0.064. \qquad (A9c)$$

Therefore the only decay of D^{*0} competing with $D^{*0} \to D^0 + \pi^0$ is the radiative transition $D^{*0} \to D^0 + \gamma$. Experimentally we have[57]

$$B(D^{*0} \to D^0\gamma) \cong 1 - B(D^{*0} \to D^0\pi^0) = 0.45 \pm 0.15. \qquad (A10)$$

The radiative decay of D^{*+} into $D^+\gamma$ has not yet been definitely observed. To obtain some feeling
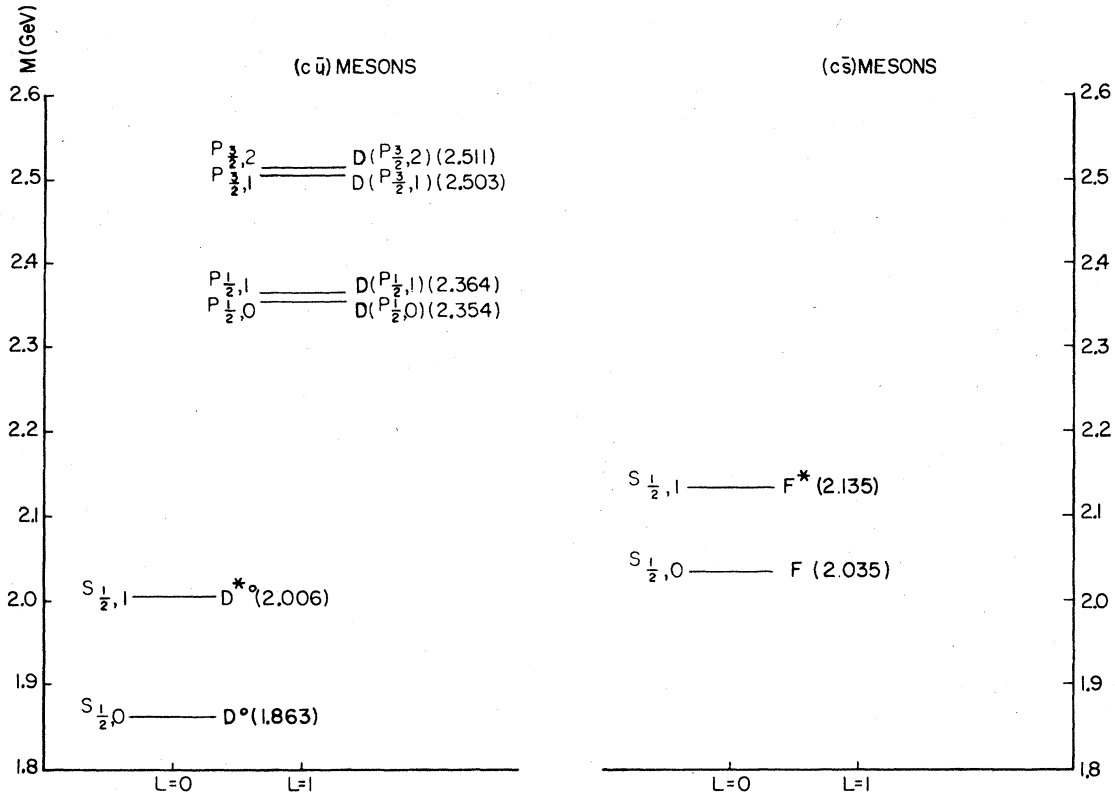
FIG. 18. Theoretical mass spectrum of charmed mesons including multiplet splittings. Notation is the same as in Fig. 16. The masses of D^{*0} and D^0 are the experimental values.

TABLE XIV. Decays of charmed mesons. Relative rates are very sensitive to phase space. Errors in p^3, due to uncertainty in charmed-meson masses, are not included.

Mode	p (MeV)	Predicted[a] rate (keV)	Predicted branching ratio (%)	Experimental branching ratio (%)
$D^{*0} \to D^0 \gamma$	137.8	35.2	47.0	45 ± 15
$D^{*0} \to D^0 \pi^0$	45.3	43.4	53.0	55 ± 15
$D^{*+} \to D^+ \gamma$	135.3	2.4[b]	3.1	
$D^{*+} \to D^+ \pi^0$	36.6	22.2	28.5	
$D^{*+} \to D^0 \pi^+$	38.9	53.4	68.5	
$F^{*+} \to F^+ \gamma$	97.6	0.32[c]	100	

[a] The rate for $D^{*0} \to D^0 + \gamma$ is calculated from Eq. (A11). The rate for $D^{*0} \to D^0 \pi^0$ is calculated from Eq. (A12).

[b] The new inputs to these rates are

$$\Gamma(D^{*0} \to D^0 \gamma)/\Gamma(D^{*+} \to D^+ \gamma) = \left(\frac{m_c^{-1} + m_u^{-1}}{m_c^{-1} - (2m_d)^{-1}} \right)^2 \left(\frac{p_0}{p_+} \right)^3,$$

which is a weak consequence of Eq. (A11), phase space, and isospin invariance for $D^* \to D\pi$.

[c] The rate for $F^{*+} \to F^+ + \gamma$ is obtained from

$$\Gamma(F^{*+} \to F^+ + \gamma)/\Gamma(D^{*+} \to D^+ + \gamma) = \left(\frac{m_c^{-1} - (2m_s)^{-1}}{m_c^{-1} - (2m_d)^{-1}} \right)^2 \left(\frac{p_F}{p_D} \right)^3.$$

for its magnitude, one may resort to the standard quark-model calculation of $M1$ decay rates:

$$\Gamma(D^* \to D\gamma) = \frac{4}{3}\,\alpha\left(\frac{e_c}{2m_c} + \frac{e_q}{2m_q}\right)^2 k^3 , \qquad (A11)$$

where $m_q = m_d = 0.335$ GeV, and $m_c = 1.84$ GeV. The same formula applies to $F^* \to F\gamma$, with $m_q = m_s = 0.45$ GeV.

The D^* branching ratios determined from (A1) and (A9)–(A11) are listed in Table XIV. The small ratio of D^{*+} to D^{*0} radiative decay rates is consistent with experiment.[57] The rate for $F^{*+} \to F^+\gamma$ is also listed in Table XIV.

It is also interesting to compare these branching ratios with what one would get under the assumption that the $s\bar{u}$ system can be treated as a heavy-light system. We would expect that $\Gamma(M^* \to M\pi)$ has the form

$$\Gamma(M^* \to M\pi) = \frac{k^3}{72\pi M^{*2}}\,C^2\,\left|(M^* E_M E)^{1/2} A\right|^2, \qquad (A12)$$

where M, M^* are pseudoscalar and vector $(Q\bar{u})$ masses, C is an isospin Clebsch-Gordan coefficient, and A is an amplitude depending only on m_u in the limit $m_Q \to \infty$. [Note that the decay amplitudes calculated in the text are of the general form (A12)]. Thus, taking A from the $K^* \to K\pi$, we find

$$|A| = 47.8\ \text{GeV}^{-3/2}. \qquad (A13)$$

The $D^* \to D\pi$ rates obtained in this manner are also listed in Table XIV. The ratio of the calculated rates for $D^{*0} \to D^0 + \pi^0$ and $D^{*0} \to D^0 + \gamma$ is in good agreement with (A10).

Our estimate of the lightest charmed P-state masses is given by (A7). They will predominantly decay into two-body final states. Since there is no phase-space inhibition, their branching ratios can be estimated from isospin consideration alone

$$
\begin{aligned}
B[D^*(P_{1/2,0}) \to D^0\pi^+] &= B[D^0(P_{1/2,0}) \to D^+\pi^-]\\
&= 2B[D^*(P_{1/2,0}) \to D^+\pi^0]\\
&= 2B[D^0(P_{1/2,0}) \to D^0\pi^0]\\
&= \tfrac{2}{3}, \qquad (A14)
\end{aligned}
$$

$$
\begin{aligned}
B[D^*(P_{1/2,1}) \to D^{*0}\pi^+] &= B[D^0(P_{1/2,1}) \to D^{*+}\pi^-]\\
&= 2B[D^*(P_{1/2,1}) \to D^{*+}\pi^0]\\
&= 2B[D^0(P_{1/2,1}) \to D^{*0}\pi^0]\\
&= \tfrac{2}{3} .
\end{aligned}
$$

$D(P_{3/2,1})$ has the same decay modes as $D(P_{1/2,1})$, while $D(P_{3/2,2})$ decays to both $D\pi$ and $D^*\pi$. According to our mass estimates, Eq. (A7), the decay into $D\rho$ is kinematically forbidden for both $D(P_{3/2,1})$ and $D(P_{3/2,2})$. Estimating that $B[D(P_{3/2,2}) \to D^*\pi] \simeq 3B[D(P_{3/2,2}) \to D\pi]$, and neglecting the $D\rho$ mode, we get

$$B[D^*(P_{3/2,2}) \to D^{*0}\pi^+] \simeq 3B[D^*(P_{3/2,2}) \to D^0\pi^+] = \tfrac{1}{2} . \qquad (A15)$$

The total widths of the charmed P states may also be crudely estimated based on analogy with the measured widths of the strange P states (see Fig. 17). They have typical hadronic widths of order 50–100 MeV.

Finally, we list some of our predictions for $b\bar{q}$ mesons. In Sec. II we already gave the masses for the $b\bar{u}$ or $b\bar{d}$ mesons:

$$m(B) = 5.26\ \text{GeV} , \qquad (A16)$$

$$m(B^*) - m(B) = 50\ \text{MeV} . \qquad (A17)$$

According to the naive quark model the masses for the $b\bar{s}$ mesons are

$$m(B_s^*) \simeq m(B^*) + m(F^*) - m(D^*) \simeq 5.45\ \text{GeV} , \qquad (A18)$$

$$m(B_s^*) - m(B_s) \simeq m(B^*) - m(B) \simeq 50\ \text{MeV} . \qquad (A19)$$

Because of the small mass difference (A17), the radiative transition $B^* \to B + \gamma$ will be the only detectable decay mode for B^* mesons. The widths calculated from (A11) are

$$
\begin{aligned}
\Gamma(B^{*-} \to B^- + \gamma) &= 1.7\ \text{keV} ,\\
\Gamma(B^{*0} \to B^0 + \gamma) &= 0.5\ \text{keV} , \qquad (A20)\\
\Gamma(B_s^* \to B_s + \gamma) &= 0.2\ \text{keV} .
\end{aligned}
$$

---

*Present address: Physics Dept., Harvard University, Cambridge, Mass. 02138.

[1]E. Eichten, K. Gottfried, T. Kinoshita, K. D. Lane, and T. M. Yan, Phys. Rev. D17, 3090 (1978); 21, 313 (E) (1980).

[2]K. Gottfried, in Proceedings of the International Symposium on Lepton and Photon Interactions at High Energies, Hamburg, 1977, edited by F. Gutbrod (DESY, Hamburg, 1977).

[3]J. D. Jackson, in Proceedings of the 1977 European Conference on Particle Physics, Budapest, edited by L. Jenik and I. Montray (CRIP, Budapest, 1978), Vol. I, pp. 603–630.

[4]V. A. Novikov, L. B. Okun, M. A. Shifman, A. I. Vainshtein, M. B. Voloshin, and V. I. Zakharov, Phys. Rep. 41C, 1–133 (1978).

[5]E. Eichten, in Proceedings of the 3rd International Conference on New Results at High Energies, Vanderbilt University, 1978 (unpublished); Harvard Report No. HUTP-78/A024 (unpublished).

[6]T. Appelquist, R. M. Barnett, and K. D. Lane, Ann. Rev. Nucl. Part. Sci. 28, 387 (1978).

[7]Y. Hara, in Proceedings of the 19th International Conference on High Energy Physics, Tokyo, 1978, edited by S. Homma, M. Kawaguchi, and H. Miyazawa (Phys. Soc. of Japan, Tokyo, 1978), pp. 824—838.

[8]J. D. Jackson, C. Quigg, and J. L. Rosner, in Proceedings of the 19th International Conference on High Energy Physics, Tokyo, 1978 (Ref. 7), pp. 391—408.

[9]G. Bhanot and S. Rudaz, Phys. Lett. 78B, 114 (1978); E. C. Poggio and H. J. Schnitzer, Brandeis University reports, 1978 (unpublished).

[10]C. Quigg and J. L. Rosner, Phys. Lett. 71B, 153 (1977); M. Machacek and Y. Tomozawa, Ann. Phys. (N.Y.) 110, 407 (1978). For earlier discussions of the logarithmic potential see Yu. B. Rumer, Zh. Eksp. Teor. Fiz. 38, 1899 (1960) [Sov. Phys. JETP 11, 1365 (1960)] and Y. Muraki, Prog. Theor. Phys. 41, 473 (1968).

[11]W. Celmaster, H. Georgi, and M. Machacek, Phys. Rev. D17, 879 (1978); 17, 886 (1978); W. Celmaster and F. S. Henyey, ibid. 18, 1688 (1978); D. Pignon and C. A. Piketty, Phys. Lett. 74B, 108 (1978); Nucl. Phys. B137, 340 (1978); Phys. Lett. 81B, 334 (1979); P. Ditsas, N. A. McDougall, and R. G. Moorhouse, Glasgow report, 1978 (unpublished); D. Beavis, S-Y . Chu, B. R. Desai, and P. Kaus, Phys. Rev. D 20, 743 (1979); R. Levine and Y. Tomozawa, ibid. 19, 1572 (1979).

[12]R. Barbieri et al., Nucl. Phys. B105, 125 (1976); W. Celmaster, Phys. Rev. D 19, 1517 (1979); E. C. Poggio and H. J. Schnitzer, ibid. 20, 1175 (1979); L. Bergström, H. Snellman, and G. Tengstrand, Phys. Lett. 80B, 242 (1979).

[13]E. Eichten, K. Gottfried, T. Kinoshita, J. Kogut, K. D. Lane, and T. M. Yan, Phys. Rev. Lett. 34, 369 (1975).

[14]E. Eichten, K. Gottfried, T. Kinoshita, K. D. Lane, and T. M. Yan, Phys. Rev. Lett. 36, 500 (1976).

[15]E. Eichten and K. Gottfried, Phys. Lett. 66B, 286 (1977).

[16]Unless stated otherwise, data on the ψ family is taken from G. Feldman and M. Perl, Phys. Rep. 33C, 285 (1977).

[17]See the reviews by A. Barbaro-Galtieri and J. Kirkby in Proceedings of the International Symposium on Lepton and Photon Interactions at High Energies, Hamburg, 1977 (Ref. 2).

[18]P. A. Rapidis et al., Phys. Rev. Lett. 39, 526 (1977).

[19]S. Yamada in Proceedings of the International Symposium on Lepton and Photon Interactions at High Energies, Hamburg, 1977 (Ref. 2).

[20]G. Flügge, in Proceedings of the 19th International Conference on High Energy Physics, Tokyo, 1978 (Ref. 7), pp. 793—810.

[21]E. Bloom, report from the "Crystal Ball" experiment at SPEAR, Moriond Conference, Les Arcs, France, 1979 (unpublished).

[21a]See note added in proof.

[22]G. Feinberg and J. Sucher, Phys. Rev. Lett. 35, 1740 (1975); J. S. Kang and J. Sucher, Phys. Rev. D 18, 2698 (1978); J. Sucher, Rep. Prog. Phys. 41, 1781 (1978).

[23]C. Berger et al., Phys. Lett. 76B, 243 (1978); C. W. Darden et al., ibid. 78B, 246 (1978).

[24]J. Bienlein et al., Phys. Lett. 78B, 360 (1978).

[25]C. W. Darden et al., Phys. Lett. 78B, 364 (1978); C. W. Darden et al., ibid. 80B, 419 (1979); Ch. Berger et al., Z. Phys. C1, 343 (1979).

[26]W. R. Innes et al., Phys. Rev. Lett. 39, 1240 (1977); K. Ueno et al., ibid. 42, 486 (1979).

[27]For a comparison with the E1 rates and the spectrum predicted by a logarithmic potential, see T. Sterling, Nucl. Phys. B141, 272 (1978).

[28]T. Appelquist and H. D. Politzer, Phys. Rev. D 12, 1404 (1975); R. Barbieri, R. Gatto, and R. Kögerler, Phys. Lett. 60B, 183 (1976); R. Barbieri, R. Gatto, and E. Remiddi, ibid. 61B, 465 (1976).

[29]W. E. Caswell, G. P. Lepage, and J. Sapirstein, Phys. Rev. Lett. 38, 488 (1977).

[30]M. Chanowitz, Phys. Rev. D 12, 918 (1975); L. Okun and M.Voloshin, Moscow Report No. ITEP-95-1976 (unpublished); S. J. Brodsky, T. A. DeGrand, R. R. Horgan, and D. G. Coyne, Phys. Lett. 73B, 203 (1978); K. Koller and T. Walsh, ibid. 72B, 227 (1977); H. Fritzsch and K.-H. Streng, ibid. 74B, 90 (1978).

[31]The value of $\alpha_s(Q^2)$ from lepton production data is expressed in terms of a scale factor Λ, and (2.22) corresponds to $\Lambda = 0.53$ GeV. Different experiments and analyses yield values of Λ that range from 0.3 to 0.75 GeV; for a review, see P. Bloch and L. Myrianthopoulos, California Institute of Technology workshop, 1979 (unpublished).

[32]K. Gottfried, Phys. Rev. Lett. 40, 598 (1978); M. B. Voloshin, ITEP report, Moscow, 1978 (unpublished); G. Bhanot, W. Fischler, and S. Rudaz, Nucl. Phys. B155, 208 (1979); M. E. Peskin, ibid. B156, 365 (1979); G. Bhanot and M. E. Peskin, ibid. B156, 391 (1979).

[33]Nevertheless, see the earlier work by R. Carlitz and M. Kislinger, Phys. Rev. D 2, 336 (1970); A. LeYaouanc, L. Oliver, O. Péne, and J. C. Raynal, ibid. 8, 2223 (1973); M.Bohm, H. Joos, and M. Krammer, Nucl. Phys. B69, 349 (1974); Acta Phys. Austriaca Suppl. XI, 3 (1973). For a model-independent analysis of ψ (3772) see G. L. Shaw and J. S. Ball, Phys. Rev. D 18, 943 (1978).

[34]G. Goldhaber et al., Phys. Lett. 69B, 503 (1977).

[35]The masses of the charmed mesons are taken from Refs. 16 and 20.

[36]L. B. Okun and M. B. Voloshin, Pis'ma Zh. Eksp. Teor. Fiz. 23, 369 (1976) [JETP Lett. 23, 333 (1976)]; A. De Rújula, H. Georgi, and S. L. Glashow, Phys. Rev. Lett. 38, 317 (1976); M. Bander, G. L. Shaw, P. Thomas, and S. Meshkov, ibid. 36, 695 (1976); C. Rosenzweig, ibid. 36, 697 (1976); A. De Rújula and R. L. Jaffe, in Experimental Meson Spectroscopy 1977, proceedings of the Vth International Conference, Boston, edited by E. von Goeler and R. Weinstein (Northeastern Univ. Press, Boston, 1978); F. Gutbrod, G. Kramer, and Ch. Rumpf, Z. Phys. C1, 391 (1979).

[37]As for ordinary baryons, $e^+e^- \to$ charmed baryons is expected to constitute only a few percent of the total charm component.

[38]One consequence of the $\gamma c\bar{c}$ coupling that underlies all charm production is that $D_1\bar{D}_2$ and $F_1\bar{F}_2$ states must be isoscalars, broken only by the mass differences in the quark isodoublets.

[39]There is an error in the definition of f^2 given by Eq. (3.42) of I. It should be replaced by the one given here.

[40]A. De Rújula, H. Georgi, and S. L. Glashow, Phys. Rev. Lett. **37**, 398 (1976).

[41]K. D. Lane and E. Eichten, Phys. Rev. Lett. **37**, 477 (1976).

[42]A. Le Yaouanc et al., Phys. Lett. **B71**, 397 (1977).

[43]The ratio R given by Eq. (5.2) is proportional to two factors of the wave function at origin, and therefore it suffers the same "radiative" correction as Γ_{ee}. We have included the correction factor $(1 - 4\kappa/\pi)$ to Eq. (5.2) in computing R.

[44]G. Feldman, in *Proceedings of the 19th International Conference on High Energy Physics, Tokyo, 1978* (Ref. 7), pp. 777–789.

[45]J. Kirz, in *Proceedings of the 19th International Conference on High Energy Physics, Tokyo, 1978* (Ref. 7), pp. 249–251.

[46]R. Brandelik et al., Phys. Lett. **76B**, 361 (1978).

[47]J. Burmester et al , Phys. Lett. **66B**, 395 (1977).

[48]W. Bacino et al., Phys. Rev. Lett. **41**, 13 (1978).

[49]W. Bacino et al., Phys. Rev. Lett. **40**, 671 (1977).

[50]See E. Eichten, in *Weak and Electromagnetic Interactions at High Energies*, proceedings of the NATO Advanced Study Institute, Cargèse, 1975, edited by M. Levy, J.-L. Basdevant, D. Speiser, and R. Gast-mans (Plenum, New York, 1976), Part A.

[51]Recent study [E. Eichten and F. Feinberg, Phys. Rev. Lett. **43**, 1205 (1979)] shows that there is no such simple relationship between confining potential and tensor force in QCD. Our discussion here is heuristic; its only purpose is to indicate how large (or small) the effect might be.

[52]Because of phase space, these numbers should be compared with data at 4.028 GeV which may not necessarily coincide with the peak of our $3S$ state.

[53]S.-H. H. Tye, Phys. Rev. D **13**, 3416 (1976); R. C. Giles and S.-H. H. Tye, ibid. **16**, 1079 (1977).

[54]The form of (A2) is justified by the recent work of E. Eichten and F. Feinberg (Ref. 51) on spin-dependent forces in QCD if both m_q and m_Q are heavy and $m_q \ll m_Q$.

[55]See, for example, A. De Rújula, H. Georgi, and S. L. Glashow, Phys. Rev. D **12**, 147 (1976).

[56]For a review of the status of meson spectroscopy, see D. W. G. S. Leith, in *Experimental Meson Spectroscopy 1977* (Ref. 36).

[57]G. Feldman, in *Quark Spectroscopy and Hadron Dynamics*, proceedings of SLAC Summer Institute on Particle Physics, 1977, edited by M. Zipf (SLAC, Stanford, 1977).